Accepted Manuscript

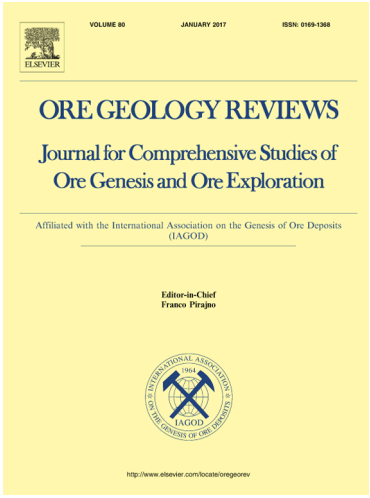

Intrusion-related gold-bismuth deposits of North-East Russia: PTX parameters and sources of hydrothermal fluids

Olga V. Vikent'eva, Vsevolod Yu. Prokofiev, Gennadiy N. Gamyanin, Nikolay A. Goryachev, Nikolay S. Bortnikov

PII: S0169-1368(18)30130-6
DOI: https://doi.org/10.1016/j.oregeorev.2018.09.004
Reference: OREGEO 2683

To appear in: *Ore Geology Reviews*

Received Date: 13 February 2018
Revised Date: 18 August 2018
Accepted Date: 5 September 2018

Please cite this article as: O.V. Vikent'eva, V. Yu. Prokofiev, G.N. Gamyanin, N.A. Goryachev, N.S. Bortnikov, Intrusion-related gold-bismuth deposits of North-East Russia: PTX parameters and sources of hydrothermal fluids, *Ore Geology Reviews* (2018), doi: https://doi.org/10.1016/j.oregeorev.2018.09.004

Intrusion-related gold-bismuth deposits of North-East Russia: PTX parameters and sources of hydrothermal fluids

Olga V. Vikent'eva[a*], Vsevolod Yu. Prokofiev[a], Gennadiy N. Gamyanin[a], Nikolay A. Goryachev[b], Nikolay S. Bortnikov[a]

[a]Institute of Geology of Ore Deposits, Petrography, Mineralogy and Geochemistry, Russian Academy of Sciences (IGEM RAS), 35 Staromonetny per., Moscow 119017, Russia

[b]North East Interdisciplinary Scientific Research Institute, Far East Branch of the Russian Academy of Sciences (NEISRI FEB RAS), 16 Portovaya Ul., Magadan 685000, Russia

ABSTRACT

Intrusion-related Au-Bi deposits of North-East Russia are related to Late Mesozoic orogenic S- and I-type granites of ilmenite series. The studied deposits differ in their position relatively to the plutons, alteration, ore body morphology and sulphide content in ores. Based on mineral composition of ores, studied deposits are divided into bismuth-sulphotelluride-quartz, bismuth-arsenide-sulpharsenide and bismuth-siderite-polysulphide types. Bismuth-sulphotelluride-quartz deposits (Levo-Dybinskoe, Kurum, Ergelyakh, Tuguchak, Basugunya) are characterised by low-sulphide (≤3 vol.%) mineralisation. Native gold associates with bismuth minerals (bismuthinite, sulphotellurides and tellurides, maldonite, jonassonite, native bismuth). Bismuth-arsenide-sulpharsenide deposits (Myakit, Chepak, Dubach, Chistoe, Kandidatskoe) host As-rich mineralisation. Löllingite and arsenopyrite are main minerals, and their contents vary from 5 to 60 vol.% (commonly ~10%). The intergrowths of native gold with bismuth minerals (sulphotellurides, tellurides, native bismuth) occur mainly in arsenopyrite. Bismuth-siderite-polysulphide (Arkachan) type is characterised by high-sulphide (5-15 vol.%) and high-carbonate (up to 35 vol.%) ores. Native gold associates with bismuthinite and other sulphobismuthites. Minerals of tellurium are rare. Fluid inclusion and stable isotope study of samples from eighteen Au-Bi deposits constrains the fluid composition, formation temperatures, pressures, and fluid sources. Four types of fluid inclusions (FI) were revealed: (I) two-phase FI, consisting of H_2O liquid and CO_2 vapour, and three-phase FI with H_2O liquid, CO_2 vapour and CO_2 liquid; (II) vapour-rich CO_2 one- or two-phase FI with minor (rarely dominant) CH_4 and N_2, sometimes with a thin liquid rim; (III) two-phase liquid-vapour aqueous inclusions; (IV) three- or multiphase FI, consisting of H_2O liquid, gas bubble and one or more daughter minerals. Au-Bi mineralisation formed at 437 to 200°C (mainly from 400 to 250°C) and 0.1

to 1.9 kbar from a H_2O-CO_2-NaCl fluid, which forms an immiscible brine and CO_2-bearing vapour at low pressure (≤1.3 kbar) as well as low- to moderate salinity CO_2-H_2O mixtures without brines at higher pressure (≥1.3 kbar). The studied deposits formed at shallow (Ergelyakh, Tuguchak, Arbatskoe at 1-2 km, Kurum, Levo-Dybinskoe at 2-3 km) and deep (Chuguluk, Shkolnoe, Arkachan at ~4 km, Dubach at >5 km) depth. Bismuth-sulphotelluride-quartz deposits commonly occur at shallow depth, whereas bismuth-arsenide-sulpharsenide and bismuth-siderite-polysulphide deposits are mainly formed in deeper environment. The stable isotope data suggest predominantly magmatic source of gold-bearing fluids, but magmatic fluid was enriched in light O, C and S isotopes as a result of fluid immiscibility. The magmatic source is consistent with the overlap in lead isotope compositions of ores and related intrusions, as well as synchronism of magmatism and hydrothermal activity according to geochronology data.

Keywords: intrusion-related gold deposits, bismuth, quartz, fluid inclusion, stable isotope, fluid immiscibility

1. INTRODUCTION

Intrusion-related gold deposits were recognised as economically important deposit type at the end of the 20th century (e.g., Thompson et al., 1999; Lang and Baker, 2001; Thompson and Newberry, 2000; Hart, 2005; Hart et al, 2002). Many deposits of this type are spatially associated with mid-Cretaceous magmatic suites of the Tintina Gold Belt in Alaska and Yukon (Smith et al., 1999; Hart et al., 2002). General features of such deposits are spatial and/or temporal relationships with moderately reduced I-type intermediate to felsic intrusions, Au-Bi-Te-W-Mo-As-Sb mineral association with low sulphide content (<5 vol.%) and reduced assemblages, as well as common metal and deposit style zoning relative to granitoid pluton (Thompson et al., 1999).

The composition, origin and evolution of hydrothermal fluids in intrusion-related gold systems were extensively debated (e.g., Thompson et al., 1999; Baker and Lang, 2001; Baker, 2002; McCoy et al., 1997; Audetat et al., 2008; Yardley and Bodnar, 2014). Magmatic (e.g., Hedenquist and Lowenstern, 1994; Newberry et al., 1995; McCoy et al., 1997), or additional metamorphic (e.g., Moravek, 1995) and meteoric (e.g., Nie et al., 2004) sources were proposed. In recent years, multiple fluid source with dominant magmatic input was recognised for these deposit styles (e.g., Baker et al., 2005; Bortnikov, 2006; Goryachev and Pirajno, 2014; Vikentyev et al., 2017; Vikent'eva et al., 2017).

Fluid inclusions and stable isotopes were studied for samples from 18 Au-Bi deposits of North-East Russia for systematic comparison with respect to type and age of

mineralisation, depth of emplacement, and proximity to the source pluton. Gold grade varies from 0.1 to 100 g/t and averages 2 to 5 g/t. Endowment of each deposit typically exceeds 50 t of gold. Thus, intrusion-related Au-Bi deposits of North-East Russia are highly promising to host large tonnage with low grade.

2. METHODS

Petrographic examination and microthermometric analysis of fluid inclusions (FI) were carried out in IGEM RAS. Individual inclusions were studied in double-polished, 100–300 μm thick sections, using a microthermometric system consisting of LINKAM THMSG 600 chamber with 50× longfocus objective lens, installed on BX-53 Olympus microscope, video camera and control computer. Samples were rapidly cooled to about −180°C to detect possible occurrence of clathrate, ice, salt hydrates, and carbonic solid phases. Upon progressive heating, up to seven phase transitions were observed in the inclusions, namely eutectic melting (T_e), melting of the carbonic phase ($T_{m(CO2)}$), melting of the ice ($T_{m(ice)}$), clathrate melting ($T_{m(clathrate)}$), homogenisation of the carbonic phase ($T_{h(CO2)}$), melting of the solid phases ($T_{m(solid)}$), mainly halite, and total homogenisation (T_h). The accuracy of temperature measurements is ±0.2 °C within a temperature interval from −60 to +60 °C, decreasing at higher and lower temperatures. The bulk salinity of the fluid was calculated from $T_{m(ice)}$ for two-phase inclusions or $T_{m(solid)}$ for multi-phase inclusions (Bodnar and Vityk, 1994), or from $T_{m(clathrate)}$ for aqueous-carbonic inclusions (Collins, 1979). Salinity of dense CH_4-N_2 fluid with $T_{m(clathrate)}$>10°C was estimated based on ice melting temperature that was corrected for H_2O content in clathrate. The predominant salt composition in aqueous solutions was identified from the melting temperature of eutectic (T_e) (Borisenko, 1977). The CO_2 concentration in the solution (C_{CO2}) was calculated based on volume and mass ratios of fluid components (Prokofiev and Naumov, 1987). Pressure was determined on the basis of the intersection of isochore and isotherm (Kalyuzhny, 1982) for syngenetic fluid inclusions. The gas mixtures were interpreted according to Kerkhof (1988) and Thiery et al. (1994). Salinity, density and pressure were estimated using FLINCOR program (Brown, 1989; Bakker, 2003). The measurements were carried out for fluid inclusions assemblages with similar phase proportions to exclude possible errors due to the necking down of the vacuoles after fluid entrapment (Roedder, 1984).

The crush-leach analysis of FI was carried out for the samples with the only dominant type of fluid inclusions at the Central Research Institute for Geological Prospecting on Base and Precious Metals (TsNIGRI). Standard technique (Kryazhev et al., 2006) includes cleaning of a sample, opening of fluid inclusions, and determination of the element composition. The ~0.5-1.0 g samples were crushed to 0.25-0.5 mm and were

cleaned by HNO_3 (50 vol. %) solution and by electrolytic and ultrasonic cleaners. Before analysis, samples were dried and then placed into a single-shot reactor, filled with helium and preheated at 110°C. Subsequent heating to 400°C and milling with corundum beads (at temperature about 120°C) allows complete opening of the inclusions. The extracted gas phase was analysed using a Tsvet-100 gas chromatograph to determine the concentration of water, CO_2, methane, and other gases. The residual liquid phase was analysed by ion chromatography (Tsvet-3006, for determination of Cl^-, F^-, SO_4^{2-}, and NO_3^-, detection limit 0.01 mg/l) and ICP-MS (Elan-6100, for determination of Br, B, Li, Rb, Cs, Sr, Ba, As, Sb, Ge, Cu, Zn, Cd, Pb, Au, Ag, Bi, Mo, W, Sn, Tl, Hg, Co, Ni, Cr, V, U, Mn, Fe, Th, Si, Te, Se) after centrifugation and addition of 7 ml of ultrapure deionised water. Calculation of fluid composition includes: (1) subtraction of the element contents in the used water from the extract analysis; (2) subtraction of the element contents in the blank extract from the working extract analysis; (3) calculation of the element mass in a quartz sample; (4) calculation of element concentrations in solutions of inclusions (normalisation on H_2O); (5) calculation of HCO_3^- content based on balance of cations and anions. Measurement accuracy is within about 5% for ion chromatography and 0.5-2% for ICP-MS.

Stable (O, C and S) isotope compositions of quartz, carbonates and sulphides were studied at the Stable Isotopes Laboratory of the Far East Geological Institute RAS (analyst A.T. Velivetskaya) by standard techniques. About 60 samples of quartz, 30 samples of carbonates and 250 samples of sulphides from the Au-Bi deposits were analysed. Samples were prepared using conventional magnetic and heavy liquid techniques. Purity estimation of was based on microscopic and Xray powder diffraction study. The results of C, O and S isotope measurements for minerals, combined with fractionation factors and fluid inclusion homogenisation data, were used to calculate the isotopic composition of hydrothermal fluid according to the equations of fractionation in hydrothermal systems (Ohmoto and Rye, 1979; Zhang et al., 1989; Zbou and Dobos, 1995; Zheng, 1999; Li and Liu, 2006).

3. GENERAL CHARACTERISTICS OF Au-Bi DEPOSITS IN NORTH-EAST RUSSIA

The studied Au-Bi deposits occur in relation to the late Mesozoic orogenic S- and I-type granite of ilmenite series of North-East Russia (Akinin et al., 2009). Granitoid emplacement is linked to the formation of large fold belts, such as Late Jurassic to Early Cretaceous Yana-Kolyma belt, Cretaceous Oloy-Chukcha (or Arctic) and (Okhotsk-Koryak belts (Goryachev, 1998; Khanchuk, 2006; Yakubchuk, 2009) (Fig. 1). According to the geochronological data, Au-Bi deposits were formed in genetic relation to the granitoids

before the formation of orogenic gold deposits (Goryachev, 2003; Goldfarb et al., 2014; Goryachev and Pirajno, 2014). The early Late Cretaceous Au-Bi deposits of North-East Russia are closely related to the evolution of the ore-magmatic systems of the Okhotsk-Chukotka continental-margin arc (Goryachev and Gamyanin, 2006; Khanchuk, 2006). The characteristic features of the studied deposits are their relation to the granitoid pluton, high Bi content and Au-Bi correlation in ores, Au-As-Bi-W-Te±Co±Ni signature of ores and the low f_{O2} – low f_{S2} environment for mineralisation, as manifested by the presence of mineral phases, such as löllingite, pyrrhotite, native bismuth, and maldonite. Along with these similar features, there are several differences such as position of the deposit relative to the granite pluton, host rock composition, alteration, orebody morphology and sulphide content in ores.

The intrusion-related Au-Bi deposits of the Verkhoyansk-Kolyma region are subdivided into three types: Au-Bi-skarn, Au-Bi-greisen and Au-Bi-vein (Gamyanin et al., 2000; Goryachev and Gamyanin, 2006). *Skarn-type deposits* (Kandidatskoe, Arbatskoe) occur at the contact of granitoids (hornfels) with calcareous clastic rock or with limestone layers. Two types of zonal skarn are formed: 1) granodiorite – garnet-plagioclase (±scapolite) rock – garnet endoskarn – pyroxene-garnet exoskarn – tremolitic rock – marble; 2) biotitic hornfels – pyroxene-(scapolite)-plagioclase rock – pyroxene-garnet skarn – pyroxene-wollastonite skarn – marble. The arsenide-sulpharsenide, polymetallic and sulphotelluride assemblages occur as disseminated, vein-disseminated or massive ores. *Greisen-type deposits* are located in the apical part of small S-type granitoid stocks with greisen bodies under hornfels (Myakit) or with swarm of greisens veins (Chepak). Greisen bodies are commonly zonal: biotitic granite – muscovitised granite – muscovite-quartz-albite-garnet greisen – albite greisen – quartz-albite-muscovite greisen – quartz-muscovite (±tourmaline) greisen. The mineralisation occurs in the central quartz-rich part. *Vein-type deposits* (Tuguchak, Chistoe, Chuguluk, Basugunya, Ergelyakh, Nenneli, Levo-Dybinskoe, Kurum, Arkachan) are the most common. The orebodies are single veins with a thickness of 1 m and a length of ~5 m; stockwork zones with a thickness up to 30-50 m, containing of 10-20% per meter of quartz, as well as mineralised shear zones with a thickness of up to 2-3 m and a length of up to 200-300 m. Veins are accompanied by alteration halos.

Based on mineral composition of ores and, specifically, on As and S contents in ores, the studied deposits are divided into bismuth-sulphotelluride-quartz, bismuth-arsenide-sulpharsenide and bismuth-siderite-polysulphide types (Goryachev and Gamyanin, 2006). *Bismuth-sulphotelluride-quartz deposits* (Levo-Dybinskoe, Kurum, Ergelyakh, Tuguchak, Basugunya) are characterised by low-sulphide (≤3 vol.%)

mineralisation. The early arsenide-sulpharsenide assemblage contains Co and Ni minerals with wide Fe-Co-Ni isomorphism. The native gold associates with bismuth minerals (bismuthinite, sulphotellurides and tellurides, maldonite, jonassonite, native bismuth). *Bismuth-arsenide-sulpharsenide deposits* (Myakit, Chepak, Dubach, Chistoe, Kandidatskoe) characteristically contain As-rich ores. Löllingite and arsenopyrite are the main minerals, and their contents vary from 5 to 60 vol.% (commonly ~10%). The finely disseminated ("invisible") gold dominates in comparison with free native gold for this deposit type. The intergrowths of native gold with bismuth minerals (sulphotellurides, tellurides, native bismuth) occur mainly in arsenopyrite. *Bismuth-siderite-polysulphide* (Arkachan) type is characterised by high-sulphide (5-15 vol.%) and high-carbonate (up to 35 vol.%) ores. Pyrite, arsenopyrite and chalcopyrite are common sulphides. Native gold associates with bismuthinite and other sulphobismuthite. Minerals of tellurium are rare.

General characteristics of the studied Au-Bi deposits are summarised in Table 1, and geological sketches of selected deposits are shown in Fig. 2.

The majority of the studied deposits are complex hydrothermal systems. Molybdenum and tungsten deposition mostly preceded gold (and bismuth) deposition. Syn- and post-gold Ag-Pb and Ag-Sb mineralisation is a product of changes of fluid composition and ore formation conditions. The Ag-Pb-Zn- and As-Sb-bearing veins, which are peripheral to the plutons and are products of the final stages of intrusion-related hydrothermal activity, were reported for many intrusion-related gold systems (Logan et al., 2000; Maloof et al., 2001; Baker et al., 2005).

4. FLUID INCLUSION STUDY

4.1. Fluid inclusion petrography

Numerous fluid inclusions were found in the vein quartz from studied Au-Bi deposits. The fluid inclusions range from 2 to 25 μm (mainly 10 to 15 μm) in size and have irregularly, rounded or negative crystal shapes. The primary, pseudosecondary and secondary fluid inclusions were observed. Primary inclusions are distributed randomly and along the growth zones of crystal. The pseudosecondary inclusions occur as trails in healed fractures, which do not cut grain boundaries. The planes of secondary inclusions crosscut the mineral grains.

Four major types of inclusions were revealed based on phase assemblages at room (+21 °C) temperature (Fig. 3). Type I of inclusions is two-phase FI, consisting of H_2O liquid and CO_2 vapour, and three-phase FI with H_2O liquid, CO_2 vapour and CO_2 liquid. Type II is vapour-rich CO_2 one- or two-phase FI, with minor (rarely dominant) CH_4 and N_2, sometimes with a thin liquid rim. Type III of FI is two-phase liquid-vapour aqueous

inclusions. Type IV is three- or multiphase FI, consisting of H_2O liquid, gas bubble and one or more daughter minerals. The cubic crystals in such inclusions are usually halite, based on refractive index. Types II and I (or III) of fluid inclusions are often located in the same growth zone of minerals that suggests their contemporaneous entrapment. Thus, the minerals, crystallised under conditions where two immiscible fluids coexist in the system, apparently resulted from aqueous–carbon dioxide–salt fluid separation into two phases: substantially liquid and substantially gaseous.

4.2. Microthermometry

The results of the microthermometry data measured for more than 600 fluid inclusions in the selected Au-Bi deposits are shown in Table 2 and plotted in Figures 4, 5, 6.

Type I of fluid inclusions prevails at the Shkolnoe, Kurum and Arkachan deposits, and it is not discovered at the Arbatskoe, Chuguluk and Basugunya deposits. The homogenisation temperature for Type I inclusions ranges between 249 and 492°C. The inclusions contain a fluid of complex composition with eutectic temperatures (T_e) ranging from −26 to −49 °C, which are typical for Mg, Fe (Na, K)-chloride solutions (Fig. 4). The values of $T_{m(CO2)}$ for majority of FI of Type I range from –60.3 to –56.6°C. Small quantities of other gas species (*i.e.*, N_2, CH_4) decrease the melting point (–56.6°C) of pure CO_2. However, $T_{m(CO2)}$ for FI in quartz of the Kurum deposit varies from -66 to -63°C that suggests significant N_2 and CH_4 admixture. Melting temperatures of clathrate ($T_{m(clathrate)}$) vary from 0.2 to 17.6°C, corresponding to the wide salinity range of 0.4 to 26.3 wt% NaCl equiv. (Fig. 5a). There are two distinctly separate groups of inclusions among the Type I of FI (Fig. 5b): more common low-salinity (<10 wt% NaCl equiv.) and moderate-salinity (>10 wt% NaCl equiv.; Arkachan and Teutedjak). A positive correlation between homogenisation temperature and salinity was determined for low-salinity FI, while this correlation is negative for moderate-salinity FI of Type I. The density of the fluid is 0.7–1.1 g/cm^3. The pressure, estimated by syngenetic Type I and II inclusions, ranges from 310 to 1910 bar (Fig. 6). The FIs of Type I contain 1.3-7.0 mol of CO_2 per kg of solution and 0.4-2.5 mol of CH_4 per kg of solution.

Type II of fluid inclusions is common for studied deposits, except Basugunya deposit (Table 2) and is dominant at the Kurum, Levo-Dybinskoe and Dubach deposits. The melting temperature of CO_2 ($T_{m(CO2)}$) varies from −63.1 to −57.5°C. This fact indicates variable concentrations of N_2 and/or CH_4 within this inclusion type. At the Kurum and Dubach deposits, phase transitions in gaseous inclusions of the Type II occur at temperatures ranging from –149.2 to –77.8°C that suggests a N_2, CH_4 or CH_4-N_2

composition of these low density (0.1-0.3 g/cm^3) inclusions. The CO_2-rich inclusions from other deposits differ in density: 0.4-0.9 g/cm^3 and about 0.1 g/cm^3. The Type II of FI with thin H_2O-NaCl (T_e of –28 to –32°C) liquid rim homogenised to vapour at 385-334°C, were found at the Tuguchak and Kurum deposits.

Type III of fluid inclusions is found almost in all studied deposits, except Shkolnoe. This inclusion type dominates at the Ergelyakh, Tuguchak, Arbatskoe and Kurum deposits. The inclusions contain a fluid of complex composition with eutectic temperatures (T_e) from −23 to −54°C, indicating the presence of Mg^{2+}, Fe^{2+}, Fe^{3+}, Ca^{2+} and K^+ cations in Na-chloride solution (Fig. 4). The fluid composition varies for different deposits: NaCl-KCl solutions are dominant at the Kurum, Mg- and Fe-rich fluids are found at the Levo-Dybinskoe and Ergelyakh, Ca^{2+} in chloride solutions is determined at the Tuguchak. Final ice melting temperatures ($T_{m(ice)}$) range between −29.7 and −0.6°C, equivalent to salinities of 1.1–23.6 wt% NaCl (commonly up to 9.0 wt% NaCl equiv.). The homogenisation temperature ranges from 383 to 189°C. The density of the fluid is 0.6–1.0 g/cm^3. The pressure, estimated by syngenetic Type III and II inclusions ranges from 90 to 1410 bar (mainly 200-400 bar) (Fig. 6). The secondary FI of Type III often occur in studied samples. These inclusions homogenise at lower temperature (from 272 to 196°C) and have similar salinity (4.5-22.6 wt% NaCl equiv.) and solution composition (T_e from -53 to -25°C) with primary inclusions. More saline fluid, trapped in secondary fluid inclusions, was found at the Arkachan and Kurum deposits, while for the Chuguluk deposit salinity of secondary inclusions decreases.

Type IV of fluid inclusions is found at the Levo-Dybinskoe, Ergelyakh, Arbatskoe, Chuguluk, Tuguchak deposits and also at the Chepak and Teutedjak deposits (Gamyanin et al., 2011; Struzhkov et al., 2008). Most inclusions of Type IV exhibit uniform eutectic temperatures, ranging from −60 to −50°C, indicating the dominance of Ca^{2+} cations in the solutions, but T_e is −10°C for skarns of the Arbatskoe deposit, suggesting a composition in the KCl-H_2O system (Fig. 4). The halite dissolution temperature in these inclusions varies from 181 to 443°C (values close to 400°C are observed at the Tuguchak, Chuguluk deposits and skarns of the Arbatskoe deposit). Total homogenisation of the Type IV inclusions occurs between 188 and 680°C (commonly 300-400°C). Salinity was estimated using the method of Bodnar and Vityik (1994), based on halite dissolution; it ranges from 29.3 to 52.4 wt% NaCl equiv. (Fig. 5). The density of the fluid is 0.8–1.3 g/cm^3.

4.3. Crush-leach analysis

The reconstructed fluid composition based on crush-leach analysis (n=50 for ore vein quartz and n=20 for magmatic quartz from the Chuguluk, Ergelyakh, Kurum and Dyby

granitoid plutons) for selected samples is shown in Table 3. Gas chromatography revealed that CO_2 was a major volatile component trapped in fluid inclusions (Fig. 7a). However, high CH_4 content in fluids was determined at the Dubach, Kurum and Chepak deposits. Na and Ca or Na and K dominate in fluids for bismuth-sulphotelluride-quartz deposits, while Na prevails for bismuth-arsenide-sulpharsenide and bismuth-siderite-polysulphide deposits. At the Chistoe and Arkachan deposits solutions are Li-enriched. Chlorine-ion is abundant at Au-Bi deposits, but HCO_3^--rich fluids were predominant for the Tuguchak, Kandidatskoe, Kurum, Nenneli and Arkachan deposits (Fig. 7b). Fluorine-ion was determined only at the Arkachan, Delyankir and Basugunya deposits, and SO_4^{2-} is common at the Chuguluk, Nenneli, Delyankir and Basugunya deposits. Common components in fluid are B (32.4 to 2603 ppm (14551 ppm, Levo-Dybinskoe)), As (11.3 to 25658 ppm), Sb (1 to 16583 ppm), Li (0.02 to 2441 ppm), Rb (0.14 to 82 ppm), Cs (0.04 to 55 ppm (192 ppm, Chuguluk)), Sr (0.15 to 652 ppm (2563 ppm, Ergelyakh)), Tl (0.01 to 12.4 ppm). Sb, As and B are significant fluid components. Br (7.6 to 877 ppm (3215 ppm, Levo-Dybinskoe)), Ba (0.07 to 302 ppm), Ge (0.05 to 12.2 ppm), Cu (0.03 to 296 ppm), Zn (2.6 to 1505 ppm), Cd (0.01 to 8 ppm (16 ppm, Chuguluk)), Mo (0.01 to 40 ppm), W (0.01 to 69 ppm (1652 ppm, Chistoe)), Co (0.01 to 4.2 ppm), Ni (0.2 to 374 ppm), Mn (0.03 to 1596 ppm) were identified in 50-90% of analyses. Other elements were determined in less than 50% of analyses: Pb (0.09 to 58 ppm), Au (0.01 to 11.3 ppm), Ag (0.01 to 3.7 ppm), Bi (0.01 to 190 ppm), Sn (0.02 to 111 ppm), Hg (0.04 to 6.9 ppm), Cr (0.02 to 53.7 ppm), V (0.06 to 10.3 ppm), U (0.01 to 1.14 ppm), Fe (2.4 to 397 ppm (up to 4896 ppm, Henneli, Galechnoe, Chuguluk, Levo-Dybinskoe)), Th (0.01 to 0.17 ppm), Si (44.8 to 10418 ppm).

4.4. Fluid inclusions in magmatic rocks

The fluid specialisation of ilmenite-bearing I- and S-types of the collision granites and magnetite-bearing I-type of the subduction-related granites from North-East Russia, which associate with gold deposits, including Myakit, Burgagu, Delyankir and Basugunya plutons, was studied (Goryachev and Berdnikov, 2006). It was determined that early high temperature fluid inclusions contain brine (crystal-fluid inclusions) and aqueous-carbon dioxide solution with a salt admixture, while late low temperature fluid inclusions contain diluted solutions. Recrystallised melt inclusions were homogenised at 805-780°C, crystal-fluid inclusions homogenised at 600°C and higher, primary fluid inclusions did so between 530 and 225°C, and secondary fluid inclusions homogenised at 370 to 155°C. Chlorides of Na and K dominate in the solutions, whereas Li, Mg, and Ca chlorides are minor. Carbon dioxide, mixed with methane and nitrogen, is a distinctive feature of the fluid, derived from only ilmenite-series granites. The aqueous-chloride solutions with insignificant CO_2 are

common for a fluid, derived from magnetite-series granite. Gaseous inclusions in quartz from the I-type granite contain CH_4 and N_2. CO_2-rich and recrystallised melt inclusions are located in the same growth zone of minerals that suggests their contemporaneous entrapment and magmatic CO_2 signature. The study of fluid inclusions in minerals of granitoids from the diorite-granodiorite plutons suggests evolution of postmagmatic fluids with decreasing temperature and pressure from high-temperature gas fluids through brine-melts to brines and dilute solutions (Goryachev and Goncharov, 1995). Increased chlorine contents in the accessory apatite correspond to increased chlorine contents in the fluids. In addition, large scale separation of CO_2-rich aqueous fluid during the final stage of magmatic evolution was determined. These fluids were responsible for major gold mineralisation.

5. STABLE ISOTOPE STUDY

5.1. Oxygen isotopes in quartz

The $\delta^{18}O$ values in quartz of studied Au-Bi deposits vary from +10.3 to +15.4‰ and fall into a narrow interval (~2‰) for each individual deposit (Fig. 8a, Tabl. 4). Quartz of the Arkachan deposit (bismuth-siderite-polysulphide type) is enriched in heavy oxygen isotope. The ^{18}O-enrichment of late quartz, coexisting with Au-Ag-Sb mineralisation (+16.2‰ Shkolnoe, +13.3 to 13.6‰ Ergelyakh), is found. At the Arkachan deposit, quartz of the later Ag-Pb mineralisation is enriched in heavy oxygen isotope (+16.3‰), but quartz of postdated Ag-Sb mineralisation is ^{16}O-enriched (~+9‰). The calculated $\delta^{18}O$ values of the ore-forming fluid in equilibrium with quartz at 300-350°C range between +4.5 and +9.4‰ (mainly +4.5 to +6.5‰, Fig. 8b). Late low-temperature Ag-Sb mineralisation is formed from fluids, enriched in light oxygen isotope ($\delta^{18}O$: 4±0.1‰ Ergelyakh, –0.5 to 0‰ Arkachan). Additionally, at the Ergelyakh and Galechnoe deposits, wolframite with $\delta^{18}O$, equal to +3‰, was studied, corresponding to fluid isotope composition of about +5.5‰. The $\delta^{18}O$ values in quartz from granite, granodiorite, aplite and pegmatite of granitoid plutons vary from +8 to +11‰ (+9.1 to +10.5‰ Chuguluk, +8.2 to +8.7‰ Ergelyakh, 8.0 to 8.9 ‰ Kurum and 8.3 to 11.2‰ Dyby plutons).

5.2. Oxygen and carbon isotopes in carbonates

Carbonates are rare in studied Au-Bi deposits, except Arkachan with up to 35 vol.% of carbonate in the veins. Early siderite and ankerite from the Arkachan deposit and late calcite from some other deposits were studied. The oxygen isotope value for studied carbonates reveals a wide range, with two distinguishing groups ($\delta^{18}O$ varies from +0.3 to +5.7‰ and from +11.7 to +15.5‰). The $\delta^{13}C$ values of carbonates fall in the narrow

interval between –7.3 and –3.6‰ (Fig. 9). The values of $\delta^{18}O$ for fluids, coexisting with carbonates from the Levo-Dybinskoe and Kandidatskoe deposits, change from +5.3 to +7.6‰ (280°C), while for Ergelyakh and Chistoe deposits these values are notably lower (–7.2 to –1.8‰). The values of $\delta^{13}C_{CO2}$ range from –5.5 to –2.7‰. The $\delta^{18}O$ and $\delta^{13}C$ values of the ore-forming fluid from Arkachan deposit range from +6.5 to +11‰ and –7.8 to –2.1‰ at 265-300°C, respectively (Gamyanin et al., 2015). The fluid, coexisting with late carbonates from Ag-Sb stage, is relatively ^{12}C-enriched (–10.3‰, Ergelyakh) or ^{12}C-depleted (–2.2±0.1‰, Arkachan).

5.3. Sulphur isotopes in sulphides

Sulphur isotope composition of sulphides for almost all above-mentioned Au-Bi deposits was studied. Arsenopyrite is the most abundant measured sulphide, but pyrrhotite, pyrite, molybdenite, chalcopyrite, sphalerite and galena were also studied. The $\delta^{34}S$ values reveal a very wide range from –18.0 to +15.8‰ (Fig. 10). The variations of sulphur isotope composition of sulphides correlate with the mineral composition type of studied deposits. The ^{34}S-enrichment of sulphides increases from the bismuth-arsenide-sulpharsenide deposits (–18.0 to –4.9‰) through the bismuth-sulphotelluride-quartz deposits (–12.5 to +4.6‰) to the bismuth-siderite-polysulphide deposits (–1.9 to 15.8‰). The $\delta^{34}S$ values of accessory sulphides from granitoids of Kurum, Ergelyakh and Basugunya plutons range from –7.6 to 0‰. Calculated $\delta^{34}S$ of fluid, equilibrated with early sulphides at 300-350°C, varies from –19.0 to +3.5‰. Ore forming fluid of the bismuth-arsenide-sulpharsenide deposits was more ^{32}S-enriched (–19.0 to –4.5‰), comparing to the bismuth-sulphotelluride-quartz deposits (–13.5 to +3.5‰) and the bismuth-siderite-polysulphide deposit (–7.0 to +6.0‰). Late sulphides were crystallised from the hydrothermal fluid with relatively heavier sulphur isotopic composition: –5.5‰, from –4.6 to –1.5‰ and from –2.0 to +14.8‰, respectively, in the above mentioned deposit type. Previous studies (Gamyanin et al., 2015) have shown that the range of $\delta^{34}S_{H2S}$ values narrows (close to 0‰) with increasing depth at the Arkachan deposit.

6. DISCUSSION

6.1. Fluid immiscibility

Three fluids (H_2O-NaCl-CO_2, CO_2-(CH_4, N_2) and H_2O-NaCl) were revealed in the studied fossilised Au-Bi hydrothermal systems. CO_2±CH_4±N_2 inclusions coexist with H_2O-NaCl inclusions in the Ergelyakh, Arbatskoe and Chuguluk deposits. Probably, they are end-member fluids of a primary low-salinity mixed H_2O-CO_2-NaCl fluid, formed during fluid immiscibility. Their coexistence with H_2O-CO_2-NaCl inclusions, displaying variable CO_2

concentrations, can be explained by the entrapment of the heterogeneous aqueous and carbonic end-member fluids. The appearance of the parent H_2O-CO_2-NaCl fluid in the same assemblages as the two immiscible phases at the Levo-Dybinskoe, Kurum and Tuguchak deposits implies that these fluid inclusions were trapped along or close to the solvus. The absence of the parent fluid phase in inclusion assemblages from the Arbatskoe and Chuguluk deposits suggests that inclusions were trapped exclusively below the solvus. At the Dubach, Shkolnoe and Arkachan deposits, CO_2-rich and H_2O-CO_2-NaCl inclusions are located in the same growth zone of quartz that suggests their contemporaneous trapping. Thus, in the hydrothermal system there were two coexisting immiscible fluids formed as a result of H_2O-CO_2-NaCl fluid separation into two phases: substantially liquid and substantially gaseous due to temperature and/or pressure drop at the deposition site.

Secondary brine (Type IV, 32.3-34.4 wt.% NaCl equiv., Levo-Dybinskoe) and mixed-salinity (1.9-20.4 wt.% NaCl equiv.) H_2O-NaCl inclusions (Type III) (T_h = 183-272°C) were found in the bismuth-sulphotelluride-quartz deposits (Tuguchak, Levo-Dybinskoe, Ergelyakh, Chuguluk, Kurum), and they possibly represent the late fluids.

6.2. PTX parameters of ore formation

Temperature

The homogenisation temperatures measured for the associations of fluid inclusion Types I and II with similar phase ratios correspond to the two-phase liquid-vapour equilibrium curve in the H_2O–CO_2–NaCl system (Bowers and Helgeson, 1983; Schmidt and Bodnar, 2000). The T_h values obtained for such heterogenic aqueous-carbonic fluid may be considered as real temperatures of mineral deposition, because pressure correction is not required in this case (Roedder, 1984). The fluid inclusion study indicates formation of the Au-Bi mineralisation at the studied deposits at 437 to 200˚C (mainly from 400 to 250°C).

In addition to the microtermometry data, the ore-forming temperature was calculated using cation (Na/K and Fe/Mn) and Si geothermometers (Díaz-Gonzáles and Santoyo, 2008; Pester et al., 2011; Fournier and Potter, 1982). The obtained values are comparable with microtermometry data (Table 4). The values of about 500°C (Si geothermometer) may be incorrect, because at temperatures >300°C high concentrations of other dissolved ions increasingly affect the silica solubility, resulting in erroneous temperature estimates using the silica geothermometer.

Pressure

Estimated fluid pressure for the studied Au-Bi deposits varies from 0.1 to 1.9 kbar (Fig. 6). Higher values of pressure were obtained for the hydrothermal systems associated with the diorite-granodiorite plutons and dykes. This fact corresponds to fluid inclusion data for magmatic quartz from the plutons. Correlation between homogenisation temperature and pressure is absent. The studied deposits formed at similar temperatures from 400 to 250°C from the fluids derived from the granitoid plutons emplaced at different depths. Late Ag-Sb mineralisation at the Shkolnoe deposit was formed at decreasing temperature and pressure, while at the Ergelyakh deposit the pressure increased during formation of late low-temperature Ag-Sb mineralisation that suggests the overpressured formation conditions (Sibson et al., 1988; Yardley et al., 2000; Cox, 2016). The fluid pressure is relatively low during fluid flow through open fractures at early stages, and it increases at late stages as a result of sealing of fractures by precipitation of hydrothermal minerals.

Pressure estimates (assuming lithostatic overburden) correspond to depths of 1 to 5 km. The studied deposits formed in shallow (Ergelyakh, Tuguchak, Arbatskoe at 1-2 km, Kurum, Levo-Dybinskoe at 2-3 km) and deeper (Chuguluk, Shkolnoe, Arkachan at ~4 km, Dubach at >5km) crust (Fig. 11). Previously, Gamyanin et al. (2003) showed that granitoids of the Ergelyakh pluton were derived from low-viscosity magma and granitoids of the Kurum pluton were derived from moderately-viscous magma. These data correspond to various conditions of crystallisation (at ≤1 kbar and 1.5-2 km for the Ergelyakh pluton; at ≥1 kbar and 3 km for the Kurum pluton) and do not contradict to our depth estimates. Mineralogical evidences of different formation depth exhibit a vertical zoning from predominantly scheelite at depth (Dubach, Sckolnoe, Arkachan) to wolframite at shallower levels (Ergelyakh, Tuguchak, Levo-Dybinskoe, Kurum). Liu and Ma (1993) demonstrated that the intrusions related to the wolframite veins were emplaced at shallow depths.

Fluid inclusion assemblages in ore quartz from the studied Au-Bi deposits depend on estimated depth of deposit formation. Namely, coexistence of brine and CO_2-rich inclusions are in deposits at shallow depth as well as presence of CO_2-rich inclusions, and lack of brines are in the deposits at deeper level (Fig. 11). This conclusion corresponds to the opinion of Bowers and Helgenson (1983), who showed that an H_2O-CO_2 fluid with a salinity of 6 wt. % NaCl equiv. (average values for magmatic fluid; 1 to 11 wt. % NaCl equiv.) will form an immiscible brine and low-salinity CO_2-bearing vapour at low pressure (<1 kbar), while at higher pressure (>1 kbar) immiscible behaviour forms low-salinity CO_2-H_2O mixtures that lack brines.

Fluid composition

Ore-forming fluid in studied hydrothermal systems is CO_2-rich. The presence of CO_2 is a ubiquitous feature of the intrusion-related gold deposits (McCoy et al., 1997; Thompson et al., 1999; Lang et al., 2000; Pirajno, 2009). Lowenstern (2001) pointed out that the presence of CO_2 can induce immiscibility both within the magmatic volatile phase and in the hydrothermal systems. At a deeper deposit (Dubach), CO_2-rich inclusions with CH_4 and N_2 admixture are dominant, while CO_2-rich inclusion and H_2O-rich brine prevail at shallow deposits (Ergelyakh, Arbatskoe) (Fig. 11). Similar correlation of fluid composition and depth was discussed by Baker and Lang, 2001; Baker, 2002. Experimental studies (Fogel and Rutherford, 1990; Blank et al, 1993) showed that CO_2-rich fluids will exsolve at higher pressures than H_2O-rich brines, because CO_2 solubility in felsic melts is one tenth that of H_2O.

Significant CH_4 and N_2 contents were determined for fluid inclusions trapped at pressure >1.5 kbar (Dublin Gulch, Scheelite Dome and MacTung deposits, Lang et al., 2000; Fort Knox, McCoy et al., 1997). Some researchers attribute presence of N_2 and CH_4 in fluid by the interaction with fluids derived from the nearby metasedimentary host rocks (Baker and Lang, 2001; Chucharro et al., 2016). It should be noted, however, that the CH_4- and N_2-rich inclusions in quartz from related I-type granite in our study suggest the magmatic fluid enrichment by these volatiles.

Halogen ratios (Br/Cl) were used to differentiate contrasting sources of salinity in fluid inclusions such as evaporated seawater, halite dissolution, or magmatic fluids (e.g., Böhlke and Irwin, 1992; Yardley et al., 2000), but the halogen ratios do not have a unique origin and similar ratios can be generated in quite different settings (Banks et al., 2000). Br/Cl (wt.) ratios for the hydrothermal fluids in studied Au-Bi deposits range from 0.001 to 0.11 (n=29), and Br is below detection limit in some hydrothermal systems (n=23, Chepak, Dubach, Shkolnoe, Kurum deposits). Some values overlap the magmatic interval (0.001 to 0.002, Böhlke and Irwin, 1992) but significant part of values exceeds it (Fig. 7c). It should be noted that Br/Cl (wt.) fluid ratios for magmatic quartz from granitoid plutons (Chuguluk, Ergelyakh, Kurum, Dyby), related to some studied deposits, range from 0.001 to 0.27 (n=14). Campbell et al. (1995) explain high halogen ratio in magmatic fluid, accompanied by high sulphate concentration due to evaporite assimilations into the magma before fluid exsolution. Br-rich magmatic fluid could be generated by magma degassing with preferential removal of Cl (as HCl) from the interacting of NaCl solutions and silica, or by the precipitation of halite from the hydrothermal fluid, resulting in a “halite effect” (Cloke and Kesler, 1979), where significant Cl is incorporated into halite and residual fluid is enriched by Br (Irwin and Roedder, 1995; Campbell et al., 2001). Moreover, Br-rich fluids within the magmatic systems could be generated as a result of crystallisation of the Cl-

bearing phases (e.g., biotite, amphibole, or apatite) prior to volatile exsolution, causing the formation of Br-enriched juvenile magmatic brines (e.g., Irwin and Roedder, 1995). High Br content of fluid entrapped by vein and magmatic quartz as well as negative correlation between Br/Cl ratios and Cl contents (Fig. 7c) suggest magmatic origin of hydrothermal fluids.

Hydrothermal fluids responsible for the formation of the studied deposits were enriched in B, As, Sb and Cl. Arsenic content is anomalously high in all intrusion-related gold systems irrespective of depth of emplacement and fluid compositions (Baker, 2002).

6.3. Sources of hydrothermal fluids

Oxygen isotope composition of fluid $\delta^{18}O_{H2O}$ equilibrated with vein quartz, wolframite and carbonate from the studied deposits varies from +4.5 to +11‰. Majority of values correspond to the typical magmatic water interval (+5 to 9‰, Ohmoto, 1986). The deposition of late quartz and carbonate from isotopically light fluid can be a result of an input of the ^{18}O depleted heated meteoric water. An isotopic shift of the fluid due to fluid immiscibility can also be responsible for this phenomenon, because the phase separation demonstrated by the fluid inclusion study may contribute to the depletion in the ^{18}O isotope in the residual fluid (Bowers, 1991).

Fluid inclusion data and mineral associations suggest that the fluid redox state was below SO_2/H_2S boundary (no sulphate minerals; presence of mineral phases such as löllingite, pyrrhotite, native bismuth, maldonite) and above CO_2/CH_4 equilibrium (the CH_4 content in fluid is mainly minor). Thus, the dominant form of carbon was H_2CO_3 (or CO_2) that implies $\delta^{13}C_{H2CO3} = \delta^{13}C_{CO2} = \delta^{13}C_{fluid}$. Also, H_2S was the dominant sulphur species in the fluid ($\delta^{34}S_{H2S} = \delta^{34}S_{fluid}$).

The $\delta^{13}C_{CO2}$ values, calculated for mineral-forming fluid equilibrated with carbonates, range from –7.8 to –2.2‰ and may indicate an input of magma- or mantle-derived carbon (Ohmoto, 1986; Jia et al., 2001). A shift toward ^{12}C-enrichment in the Arkachan deposit can be caused by abundant formation of carbonates, accompanied by CO_2-depletion in the fluid due to its incorporation in the carbonate minerals. This process can lead to enrichment of the fluid with light carbon isotope (Zbou and Dobos, 1995).

The sulphur isotope values are typically within the “magmatic” range (0±5‰) for reduced intrusion-related deposits (e.g., Newberry et al., 1995; McCoy et al., 1997), but our study shows a wider range of $\delta^{34}S_{H2S}$ (–19.0 to +3.5‰, for early sulphides, and –5.5 to +14.8‰, for late sulphides) for the Au-Bi deposits of North-East Russia. The ^{32}S-enrichment of sulphides was documented at the deposits in the Tintina Gold Province ($\delta^{34}S$: Clear Creek –12.7 to –9.5‰, Marsh et al., 2003; Scheelite Dome –10.9 to –7.1‰,

Mair et al., 2006; Donlin Creek –16 to –10‰, Goldfarb et al., 2004). Ishihara (Sasaki and Ishihara, 1979) showed two specific isotope trends: the magnetite-series granitoids all have positive $\delta^{34}S$ values from +1 to +9‰, while for the ilmenite-series rocks negative values between –11 and +1‰ are predominant. The majority of the studied deposits associates with ilmenite-series granitoids. In addition the variations in sulphur isotope composition of fluid can be explained by two processes: (1) mixing magmatic fluid with the ^{34}S-depleted fluid, and (2) the fluid immiscibility resulting in ^{32}S-enrichment of H_2S in residual fluid (Ohmoto, 1986; McKibben and Eldridge, 1990; Seal, 2006). Fluid immiscibility, accompanied by removal of reduced gas species from primary ore-bearing fluid, leads to ^{32}S-enrichment of the residual fluid that is reflected in ^{34}S-depletion of sulphides. This mechanism seems to be preferable because the fluid immiscibility was documented by the fluid inclusion study. The ^{34}S-enrichment of the late fluid at Arkachan deposit suggests a sulphur input from host rocks at the late stages.

Additionally, the magmatic source is consistent with the overlap of lead isotope compositions of ores and related intrusions (Gamyanin et al., 2003; Gamyanin, unpubl. data). Moreover, the geochronological data demonstrate that magmatism and hydrothermal activity were contemporaneous (Table 1).

7. CONCLUSIONS

Fluid inclusion and stable isotope data, presented in this paper in combination with previous geological and mineralogical studies (Gamyanin et al., 2003), were used for reconstruction of ore-forming conditions and sources of hydrothermal fluids for the intrusion-related Au-Bi deposits of North-East Russia. The studied deposits differ in their position relatively to the plutons, alteration, ore body morphology and sulphide content in ores. The change of f_{O2} – f_{S2} environment corresponds to different mineral types of the Au-Bi deposits: bismuth-arsenide-sulpharsenide, bismuth-sulphotelluride-quartz and bismuth-siderite-polysulphide deposits. The Au-Bi mineralisation was formed at 437 to 200˚C (mainly from 400 to 250°C) from H_2O-CO_2-NaCl fluid, which forms immiscible brine and CO_2-bearing vapour at low pressure (≤1.3 kbar) as well as low- to moderate salinity CO_2-H_2O mixtures without brines at higher pressure (≥1.3 kbar). Bismuth-sulphotelluride-quartz deposits commonly occur in shallow crust, whereas bismuth-arsenide-sulpharsenide and bismuth-siderite-polysulphide deposits mainly formed in deeper crust. The stable isotope data suggest predominantly magmatic source of gold-bearing fluids, but magmatic fluid was enriched in light O, C and S isotopes as a result of fluid immiscibility. Magmatic source is consistent with the overlap in lead isotope compositions of ores and related

intrusions, as well as with the synchronism of magmatism and hydrothermal activity according to geochronological data.

ACKNOWLEDGEMENTS

We thank S.G. Kryazhev, Yu.V. Vasyuta and A.T. Velivetskaya for carrying out the analytical procedures. The manuscript was significantly improved by constructive and helpful reviews from Alexander Yakubchuk and Serguei Soloviev. The study was supported by the Russian Scientific Foundation (project 14-17-00693-P, fluid inclusion study and genetic interpretation), "Far East" program of FEB RAS (project 18-2-001, field work and stable isotope study) and the basic themes of IGEM RAS.

REFERENCES

Akinin, V.V., Prokopiev, A.V., Toro, J., Miller, E.L., Wooden, J., Goryachev, N.A., Alshevsky, A.V., Bakharev, A.G., Trunilina, V.A., 2009. U–Pb SHRIMP age of granitoids from the main batholith belt (North East Asia). Dokl. Earth Sci. 426, 605–610.

Audetat, A., Pettke, T., Heinrich, C.A, Bodnar, R.J., 2008. The composition of magmato-hydrothermal fluids in barren and mineralized intrusions. Econ. Geol. 103, 877–908.

Baker, T., 2002. Emplacement depth and CO_2-rich fluid inclusions in intrusion-related gold deposits. Econ. Geol. 97, 1109–1115.

Baker, T., Lang, R.J., 2001. Fluid inclusion characteristics of intrusion-related gold mineralisation, Tombstone-Tungsten magmatic belt, Yukon Territory, Canada. Miner. Dep. 36, 563–582.

Baker, T., Pollard, P.J., Mustard, R., Mark, G., Graham, J.L., 2005. A comparison of granite-related tin, tungsten, and gold-bismuth deposits: implications for exploration. SEG Newsletter 61, 5–17.

Bakker, R.J., 2003. Package FLUIDS 1. Computer programs for analysis of fluid inclusions data and for modeling bulk fluid properties. Chem. Geol. 194, 3–23.

Banks, D.A., Green, R., Cliff, R.A., Yardley, B.W.D., 2000. Chlorine isotopes in fluid inclusions: determination of the origins of salinity in magmatic fluids. Geochim. Cosmochim. Acta. 64, 1785–1789.

Blank, J.G., Stolper, E.M., Carroll, M.R., 1993. Solubilities of carbon dioxide in rhyolite melt at 850°C and 750 bars. Earth Planet Sci. Lett. 119, 27–36.

Bodnar, R.J., Vityk, M.O., 1994. Interpretation of microterhmometric data for H_2O–NaCl fluid inclusions, in: Fluid Inclusions in Minerals: Methods and Applications, Eds. B. De Vivo and M.L. Frezzotti, Pontignano, Sienna, pp. 117–130.

Borisenko, A.S. 1977. Cryometric study of salt composition of solutions in gas–liquid inclusions in minerals, Geol. Geofiz. (8), 16–28 (in Russian).

Bortnikov, N.S., 2006. Geochemistry and origin of the ore-forming fluids in hydrothermal-magmatic systems in tectonically active zones. Geol. Ore Dep. 48 (1), 1–22.

Bowers, T.S., 1991. The deposition of gold and other metals. Pressure-induced fluid immiscibility and associated stable isotope signatures. Geochim. Cosmochim. Acta 55, 2417–2434.

Bowers, T.S., Helgeson, H.C., 1983. Calculation of the thermodynamic and geochemical consequences of nonideal mixing in the system H_2O-CO_2-NaCl on phase relations in geologic systems: Equation of state for H_2O-CO_2-NaCl fluids at high pressures and temperatures. Geochim. Cosmochim. Acta 47, 1247–1276.

Böhlke, J.K., Irwin, J.J., 1992. Laser microprobe analyses of Cl, Br, I, and K in fluid inclusions: Implications for sources of salinity in some ancient hydrothermal fluids. Geochim.Cosmochim. Acta 56, 203–225.

Brown, P.E., 1989. Flincor: A microcomputer program for the reduction and investigation of fluid inclusion data, Amer. Min. 74, 1390–1393.

Campbell, A.R., Banks, D.A., Phillips, R.S., Yardley, B.W.D., 1995. Geochemistry of Th-U-REE mineralizing magmatic fluids, Capitan Mountains, New Mexico. Econ. Geol. 90, 1271–1287.

Campbell, A.R., Lundberg, S.A.W., Dunbar, N.W., 2001. Solid inclusions of halite in quartz: evidence for the halite trend. Chem. Geol. 173(1–3), 179–191. DOI:10.1016/S0009-2541(00)00274-6.

Chicharro, E., Boiron M.-C., López-García J.Á., Barfod D.N., Villaseca C., 2016. Origin, ore forming fluid evolution and timing of the Logrosán Sn–(W) ore deposits (Central Iberian Zone, Spain). Ore Geol. Rev. 72, 896–913.

Cloke, P.L., Kesler, S., 1979. The halite trend in hydrothermal solutions. Econ. Geol. 74, 1823–1831.

Collins, P.L.P., 1979. Gas hydrates in CO_2 bearing fluid inclusions and the use of freezing data for estimation of salinity. Econ. Geol. 74, 1435–1444.

Cox, S., 2016. Injection-driven swarm seismicity and permeability enhancement: Implications for the dynamics of hydrothermal ore systems in high fluid-flux, overpressured faulting regimes. Econ. Geol. 111 (3), 559–587.

Díaz-Gonzáles, L., Santoyo, E., 2008. A new precise calibration of the Na/K geothermometer using a world database of geothermal fluids and improved geochemometric techniques. Geochim. Cosmochim. Acta 72, A215.

Fogel, R.A., Rutherford, M.J., 1990. The solubility of carbon dioxide in rhyolitic melts: a quantitative FTIR study. Am. Miner. 75, 1311–1326.

Fournier, R.O., Potter, R.W., 1982. A Revised and Expanded Silica (Quartz) Geothermometer. Geotherm. Res. Bull. 11, 3-12.

Gamyanin, G.N., Goncharov, V.I., Goryachev, N.A., 2000. Gold-rare metal deposits of Northeast Russia. Geol. Pac. Ocean 15, 619–636.

Gamyanin, G.N., Goryachev, N.A., Bakharev, A.G., Kolesnichenko, P.P., Diman, E.N., Zaitsev, A.I., Berdnikov, N.V., 2003. Conditions of Origin and Evolution of Gold Ore Magmatic Granitoid Systems in North East Asia Mesozoids. NEISRI FEB RAS, Magadan (in Russian).

Gamyanin, G.N., Prokofiev, V.Yu, Goryachev, N.A., Bortnikov, N.S., 2011. Ore-forming fluids of the gold–bismuth deposits in North-East Russia. Gold of the North Pacific Rim. II International Geology and Mining Forum dedicated to Yu.A.Bilibin's 110th anniversary. Abstracts of the Geology & Mining. NEISRI FEB RAS, Magadan. pp. 80–81.

Gamyanin, G.N., Vikent'eva, O.V., Prokof'ev, V.Yu., Bortnikov, N.S., 2015. Arkachan: A new gold-bismuth-siderite-sulphide type of deposit in the West Verkhoyansky tin district, Yakutia. Geol. Ore Dep. 57 (6), 465–495.

Goldfarb, R.J., Ayuso, R., Miller, M.L., Ebert, S.W., Marsh, E.E., Petsel, S.A., Miller, L.D., Bradley, D., Johnson, C.A., McClelland, W., 2004, The Late Cretaceous Donlin Creek gold deposit, southwestern Alaska – Controls on epizonal ore formation. Econ. Geol. 99 (4), 643–671.

Goldfarb, R.J., Taylor, R., Collins, G., Goryachev, N.A., Orlandini, O.F., 2014. Phanerozoic continental growth and gold metallogeny of Asia. Gondwana Res. 25 (1), 49–102. DOI:10.1016/j.gr.2013.03.002.

Goryachev, N.A., 1998. Geology of Mesozoic Gold–Quartz Vein Belts of Northeast Asia. NEISRI FEB RAS, Magadan (in Russian).

Goryachev, N.A., 2003. Origin of Gold Quartz Vein Belts throughout the Northern Pacific Area. NEISRI FEB RAS, Magadan (Russian).

Goryachev, N.A., 2005. The Uda-Murgal magmatic arc: geology, magmatism, metallogeny. Problems of Metallogeny of Ore Regions in the North-East Russia, Proceedings. NEISRI FEB RAS, Magadan. pp. 17–38 (in Russian).

Goryachev, N.A., Berdnikov, N.V., 2006. Types of ore-bearing granites of south-eastern part of Mesozoids of North-East Russia and their fluid specialisation. J. Geol. Pac. Ocean 25 (3), 40–52.

Goryachev, N.A., Gamyanin, G.N., 2006. Gold–bismuth (gold-raremetal) deposits of North East Russia: types, and exploration perspectives. Gold ore deposits of East Russia. NESC FEB RAS, Magadan, pp. 50–62 (in Russian).

Goryachev, N.A., Goncharov, V.I., 1995. Late Mesozoic granitoid magmatism and related gold and tin mineralisation of North-East Asia. Resour. Geol. Spec. Issue 18, 111–122.

Goryachev, N.A., Pirajno, F., 2014. Gold deposits and gold metallogeny of Far East Russia. Ore Geol. Rev. 59, 123–151.

Hart, C.J.R., 2005. Classifying, distinguishing and exploring for intrusion-related gold systems. The Gangue, Geological Association of Canada, Mineral Deposits Division Newsletter 87(1), 4–9.

Hart, C.J.R., McCoy, D., Goldfarb, R.J., Smith, M., Roberts, P., Hulstein, R., Blake, A.A., Bundtzen T.K., 2002. Geology, exploration and discovery in the Tintina gold province, Alaska and Yukon. Soc. Econ. Geol. Spec. Publ. 9, 241–274.

Hedenquist, J.W., Lowenstern, J.B., 1994. The role of magmas in the formation of hydrothermal ore deposits. Nature 370, 519–527.

Hoefs, J., 1987. Stable Isotope Geochemistry. Springer, Berlin.

Irwin, J.J., Roedder, E., 1995. Diverse origins of fluid in magmatic inclusions at Bingham (Utah, USA), Butte (Montana, USA), St Austell (Cornwall, UK) and Ascension Island (mid-Atlantic, UK) indicated by laser microprobe analysis of Cl, K, Br, I, Ba+Te, U, Ar, Kr and Xe. Geochim. Cosmochim. Acta 59, 295–312.

Jia, Y., Li, X., Kerrich, R., 2001. Stable isotope (O, H, S, C, and N) systematic of quartz vein systems in the turbidite-hosted Central and North Deborah gold deposits of the Bendigo Gold Field, Central Victoria, Australia: Constraints on the origin of ore-forming fluids. Econ. Geol. 96, 705–721.

Kalyuzhny, V.A., 1982. Principles of the Theory on Mineral-Forming Fluids. Naukova Dumka, Kiev (in Rus.).

Kerkhof, A.M., 1988. The System CO_2-CH_4-N_2 in Fluid Inclusions: Theoretical Modeling and Geological Applications. Free University Press, Amsterdam.

Khanchuk, A.I., 2006. Geodynamics, Magmatism and Metallogeny of the Russian East. Dalnauka: Vladivostok.

Kryazhev, S.G., Prokof'ev, V.Yu., Vasyuta, Yu.V., 2006. Use of method ICP MS at the analysis of composition of ore-forming fluids. Vestnik MSU, Geology. 4, 30–36.

Lang, J.R., Baker, T., Hart, C.J.R., Mortensen, J.K., 2000. An exploration model for intrusion-related gold systems. Soc. Econ. Geol. Newsletter 40, 1–15.

Lang, J., Baker, T., 2001. Intrusion-related gold systems: the present level of understanding. Mineral. Dep. 36 (6), 477–489.

Layer, P.W., Newberry, R.J., Fujita, K., Parfenov, L., Trunilina, V., Bakharev, A., 2001. Tectonic setting of the plutonic belts of Yakutia, northeast Russia, based on $^{40}Ar/^{39}Ar$ geochronology and trace element geochemistry. Geology 29, 167–170.

Li, Y.B., Liu, J.M., 2006. Calculation of sulphur isotope fractionation in sulphides. Geochim.Cosmochim. Acta 70, 1789–1795.

Liu, Y., Ma, D., 1993. Vein-type tungsten deposits of China and adjoining regions. Ore Geol. Rev. 8, 233–246.

Logan, J., Lefebure, D., Cathro, M., 2000. Plutonic-related gold-quartz veins and their potential in British Columbia, in: The Tintina Gold Belt Concepts, Exploration and Discoveries, British Columbia and Yukon Chamber of Mines, Cordilleran Exploration Roundup, Exten. Abs., Ed. J.L. Jambour. pp.197–225.

Lowenstern, J.B., 2001. Carbon dioxide in magmas and implications forhydrothermal systems. Mineral. Dep. 36, 490–502. DOI:10.1007/s001260100185

Maloof, T.L., Baker, T., Thompson, J.F.H., 2001. The Dublin Gulch intrusion-hosted gold deposit, Tombstone plutonic suite, Yukon Territory, Canada. Mineral. Dep. 36 (6), 583–593.

Mair, J.L., Goldfarb, R.J., Johnson, C.A., Hart, C.J.R., Marsh, E.E., 2006. Geochemical constraints on the genesis of the Scheelite Dome intrusion-related gold deposit, Tombstone gold belt, Yukon, Canada. Econ. Geol. 101 (3), 523–553.

Marsh, E.E., Goldfarb, R.J., Hart, C.J.R., Johnson, C.A., 2003. Geology and geochemistry of the Clear Creek intrusion-related gold occurrences, Tintina gold province, Yukon, Canada. Canad. J. Earth Sci. 40 (5), 681–699.

McCoy, D., Newberry, R.J., Layer, P., DiMarchi, J.J., Bakke,A., Masterman, S., Minehane, D.L., 1997. Plutonic-related gold deposits of Interior Alaska, in: Goldfarb, R.J., Miller, L.D. (Eds.), Mineral Deposits of Alaska, Econ. Geol. Monogr. 9, 191–241.

McKibben, M.A., Eldridge, C.A.S., 1990. Radical sulphur isotope zonation of pyrite accompanying boiling and epithermal gold deposition: a SHRIMP study of the Valles Caldera, New Mexico. Econ. Geol. 85, 1917–1925.

Moravek, P., 1995. The Mokrsko gold deposit, in: Gold deposits of the central and SW part of the Bohemian massif. Third Biennial Society for Geology Applied to Mineral Deposits Meeting, Prague 1995, Excursion guide, Ed. P. Moravek. pp. 33–61.

Newberry, R.J., McCoy, D.T., Brew, D.A., 1995. Plutonic-hosted gold ores in Alaska: Igneous vs. metmorphic origins. In: Ishihara, S., Czamanske, G.K. (Eds.), Proc. Sapporo International Conf. on Mineral Resources of the NW Pacific Rim, Res Geol, Spec Iss. 18, 57–100.

Nie, F.-J., Jiang, S.-H., Liu, Y., 2004. Intrusion-Related Gold Deposits of North China Craton, People's Republic of China. Resource Geology. 54 (3), 299–324.

Nokleberg, W.J., Bundtzen, T.K., Dawson, K.M., Eremin, R.A., Goryachev, N.A., Koch, R.D., Ratkin, V.V., Rozenblum, I.S., Shpikerman, V.I., Frolov, Y.F., Gorodinsky, M.E., Melnikov, V.D., Ognyanov, N.V., Petrachenko, E.D., Pozdeev, A.I., Ross, K.V., Wood, D.H., Khanchuck, A.I., Kovbas, L.I., Nekrasov, I.Y., Sidrov, A.A., 1996. Significant metalliferous and selected non-metalliferous lode deposits and placer districts for the Russian Far East, Alaska, and the Canadian Cordillera. U.S. Geological Survey, Open-file Report 96-513-A, p. 1–39.

Ohmoto, H., 1986. Stable isotope geochemistry of ore deposits. Rev. Mineralogy 16, 491-560.

Ohmoto, H., Rye, R.O., 1979. Isotopes of sulphur and carbon, in: Barnes, H.L., (Ed.), Geochemistry of Hydrothermal Ore Deposits, J.Willy Sons, New York, pp. 509–567.

Parfenov, L.M., Kuzmin, M.I. (Eds.), 2001. Tectonics, Geodynamics and Metallogeny of the Sakha Republic (Yakutia). MAIK "Nauka/Interperiodika": Moscow (in Russian).

Pester, N.J., Rough, M., Ding, K., Seyfried, Jr.W.E., 2011. A new Fe/Mn geothermometer for hydrothermal systems: Implications for high-salinity fluids at 13°N on the East Pacific Rise. Geochim. Cosmochim. Acta 75, 7881–7892.

Pirajno, F., 2009. Hydrothermal Processes and Mineral Systems. Springer, Berlin.

Prokof'ev, V.Yu., Naumov, V.B., 1987. Geochemical features of ore-forming solutions for the Zyryanovsk pyrite-polymetallic deposit (Rudnyi Altai). Geochemistry 3, 375-386.

Roedder, E., 1984. Fluid inclusions, in: Review in Mineralogy, Ed. P.H. Ribbe, 12. Mineralogical Society of America.

Sasaki, A., Ishihara, S., 1979. Sulfur isotopic composition of the magnetite-series and ilmenite-series granitoids in Japan. Contrib. Miner. Petr. 68, 107-115.

Seal, R.R., 2006. Sulfur isotope geochemistry of sulfide minerals. Rev. Miner. Geochem. 61, 633–677.

Schmidt, C., and Bodnar, R.J., 2000. Synthetic fluid inclusions: XVI. PVTX properties in the system H_2O-NaCl-CO_2 at elevated temperatures, pressures, and salinities. Geochim. Cosmochim. Acta. 64, 22, 3853–3869.

Sibson, R.H., Robert, F., Poulson, K.H., 1988. High-angle reverse faults, fluid pressure cycling and mesothermal gold-quartz deposits. Geology 16, 551–555.

Sheppard, S.M.F., 1986. Characterisation and isotopic variations in natural water. Rev. Mineral. 16, 165–183.

Smith, M.T., Thompson, J.F.H., Bressler, J., Layer, P., Mortensen, J.K., Abe, I., Takaoka, H., 1999. Geology of the Liese Zone, Pogo property, east-central Alaska. Soc.Econ. Geol. Newsletter 38, 1, 12-21.

Struzhkov, S.F., Kryazhev, S.G., Natalenko, M.V., Golubev, S.Yu, 2008. Contrasting fluid inclusion characteristics of the gold-quartz and gold-sulfide-quartz deposits of the Central Kolyma region (NE Russia). Proceedings of XIII International Conference on Thermobarogeochemistry and IVth APIFIS Symp., vol. 2. IGEM RAS, Moscow. 124–127 (in Russian).

Thiery, R., Kerkhof, A.M., Dubessy, J., 1994. PTX properties of CH_4-CO_2 and CO_2-N_2 fluid inclusions: modeling for T<31 °C and P<400 bars. Europ. J. Mineral. 6, 753-771.

Thompson, J.F.H., Newberry, R.J., 2000. Gold deposits related to reduced granitic intrusions. Rev. Econ. Geol. 13, 377–400.

Thompson, J.F.H., Sillitoe, R.H., Baker, T., Lang, J.R., Mortensen, J.K., 1999. Intrusion-related gold deposits associated with tungsten-tin provinces. Mineral. Dep. 34, 323–334.

Vikent'eva, O.V., Bortnikov, N.S., Vikentyev, I.V., Groznova, E.O., Lyubimtseva, N.G., Murzin, V.V., 2017. The Berezovsk giant intrusion-related gold-quartz deposit, Urals, Russia: Evidence for multiple magmatic and metamorphic fluid reservoirs. Ore Geol. Rev. 91, 837-863. DOI: 10.1016/j.oregeorev.2017.08.018

Vikentyev, I.V., Mansurov, R.Kh., Ivanova, Yu.N., Tyukova, E.E., Sobolev, I.D., Abramova, V.D., Vykhristenko, R.I., Trofimov, A.P., Khubanov, V.B., Groznova, E.O., Dvurechenskaya, S.S., Kryazhev, S.G., 2017. Porphyry-style Petropavlovskoe gold deposit, the Polar Urals: geological position, mineralogy, and formation conditions. Geol. Ore Dep. 59(6), 482–520. DOI: 10.1134/S1075701517060058

Yakubchuk, A.S., 2009. Revised Mesozoic–Cenozoic orogenic architecture and gold metallogeny in northern Circum-Pacific. Ore Geol. Rev. 35, 447–454

Yardley, B., Gleeson, S., Bruce, S., Banks, D., 2000. Origin of retrograde fluids in metamorphic rocks. J. Geoch. Explor. 69-70, 281–285.

Yardley, B.D., Bodnar, R.J., 2014. Fluids in the Continental Crust. Geochem. Perspectives 3(1).

Zbou, T., Dobos, S.K., 1995. A carbon and oxygen stable isotopic study of the siderite alteration in the Black Ridge gold deposit, Clermont, Central Queesland. Mineral. Dep. 30(1), 30–38.

Zhang, L.-G., Liu, J.-X., Zhou, H.B., Chen, Z.-S., 1989. Oxygen isotope fractionation in the quartz-water-salt system. Econ. Geol. 89, 1643–1650.

Zheng, Y.-F., 1999. Oxygen isotope fractionation in carbonate and sulfate minerals. Geochem. J. 33, 109–126.

Fig. 1. Location map of intrusion-related Au-Bi deposits of North-East Russia (modified after Goryachev and Pirajno, 2014).

Fig. 2. Geological maps of selected Au-Bi deposits of North-East Russia (modified after Goryachev, 2003): **a**, **b** – Myakit Au-Bi greisen-type deposit with two ore prospects: North (I) and South (II), after Z.I. Litovchenko (**b** – South greisen body); **c** – Ergelyakh deposit; **d** – Levo-Dybinskoe deposit with quartz stockworks (T – Tenisty area, O – Oderzhimy area), simplified after A.V. Kokin and Yu.A. Zubkov; **e**, **f** – Kurum deposit, after A.V. Kokin (**f** – interrelation of aplite, quartz and sulphide veins); **g**, **h** – Tuguchak deposit, modified after V.I. Shur (**h** – detail: transition of aplite to pegmatite and quartz veins).

Fig. 3. Photomicrographs of fluid inclusions trapped in quartz of Au-Bi deposits.

a, **b** − aqueous-carbonic inclusion, Type I (**a** − at +20°C, **b** – at −10°C); **c**, **d** – vapor-rich (CO_2±CH_4±N_2) inclusion, Type II (**c** – at +20°C, **d** – at −5°C); **e** − two-phase liquid-vapour aqueous inclusion, Type III; **f** − multiphase inclusion of chloride brine, Type IV. Scale bar is 10 mkm. **a**-**d** – Levo-Dybinskoe deposit, **e**, **f** – Tuguchak deposit.

Fig. 4. Homogenisation (T_{hom}) vs. eutectic temperatures (T_{eut}) plots for fluid inclusions (FI) in the quartz from Au-Bi deposits. **a** – summarised plot for different FI types; **b**-**d** – plots for I (**b**), III (**c**) and IV (**d**) FI types for studied deposits.

Fig. 5. Homogenisation temperature (T_{hom}) vs. salinity (C_{salt}) plots for fluid inclusions in the quartz of Au-Bi deposits. **a** – summarised plot for studied deposits; **b** – summarised plot for different FI types. Diorite and granite boxes after Goryachev and Goncharov, 1995. Au-Bi-As – bismuth-arsenide-sulpharsenide deposits, Au-Bi-Sid – bismuth-siderite-polysulphide deposits. * – data from Struzhkov et al., 2008.

Fig. 6. Pressure (P) vs. homogenisation temperature (T_{hom}) plot for fluid inclusions in the quartz of Au-Bi deposits. Diorite and granite boxes after Goryachev and Goncharov, 1995. * – data from Struzhkov et al., 2008.

Fig. 7. Fluid composition for Au-Bi deposits of North-East Russia according to crush-leach analysis. **a** – CH_4 contents vs. CO_2 contents; **b** – HCO_3 contents vs. Cl contents; **c** – Br/Cl (wt.) ratios vs. Cl contents in fluids. Blank symbols – bismuth-arsenide-sulpharsenide deposits, filled symbols – bismuth-sulphotelluride-quartz deposits, crosses – bismuth-siderite-polysulphide deposits, red symbols – quartz from granitoids.

Fig. 8. Oxygen isotopic composition of quartz (**a**) and ore-forming fluid (**b**) in comparison with a range of magmatic waters (after Sheppard, 1986) at the studied Au-Bi deposits.

Fig. 9. Summary of carbon and oxygen isotope data for vein carbonates from Au-Bi deposits in comparison with ranges of carbonatites and sedimentary carbonates (after Hoefs, 1987).

Fig. 10. Sulphur isotope compositions of sulphide minerals from ore veins of the studied Au-Bi deposits in comparison with a range of “magmatic” sulphur (after Ohmoto, 1986).

Fig. 11. A schematic model for Au-Bi deposits of North-East Russia, demonstrating relationships between fluid composition and emplacement depth of parent pluton estimated by pressure (adapted from Baker and Lang, 2001).

Table 1. General characteristics of Au-Bi intrusion-related deposits of North-East of Russia.

Deposit	Levo-Dybinskoe	Kurum	Chuguluk	Ergelyakh	Nenneli	Tuguchak
Mineral type*	Au-Bi-Te	Au-Bi-Te	Au-Bi-Te	Au-Bi-Te	Au-Bi-Te	Au-Bi-Te
Coordinates (N/E)	62.83/139.58	62°00´/139°00´	64.383/146.396	63,43/143,53	68°09´/136°38´	69°30´/149°19´
Metallogenic belt	Allakh-Yun, J_3-K_1	Allakh-Yun, J_3-K_1	Yana-Kolyma, J_3-K_1	Yana-Kolyma, J_3-K_1	Yana-Kolyma, J_3-K_1	Yana-Polousnaya, K
Pluton/ composition/type	Dyby/ granodiorite-granite/ I_{ilm}	Kurum/ granodiorite-granite/I_{ilm}	Chuguluk/granite	Ergelyakh/ granodiorite-granite	Kureninsk	Ulakhan-Siss/ granodiorite-granite
Rock surrounding pluton	Hornfelsed sandstone (P_2)	Clastic rocks (P_2)		Hornfelsed sandstone, siltstone and schist (T_3-J_1)	Sandstone and schist (J_{1-2})	Calcareous sandstone and schist (P)
Alteration	Sericitisation	Sericitisation	Greisenisation	Greisenisation		Sericitisation, silicification
Ore location	Hornfels	Apical part of massif and hornfels	Apical part of batholith and hornfels	Apical part of massif and hornfels	Hornfels	Apical part of massif
Ore bodies	Veins, stockwork	Veins	Veins	Veins, stockwork	Stockwork, veins	Veins
Mineralisation (mineral assemblages)	Q-Sch-Kfs-Ms, Q-Wf-Mo, sAs, Au-Bi-sTe	Mo-(Wf)-Ms, Q-Po-Lo-Apy, Gn-Sp-Ccp-Sch, Au-Bsm-sTe-Bi	Apy-Lo-Po-Q, Bi-sTe (Ttd, JoA, JoB, Tbs, Au), Cal	Wf-Tur-Q (NE veins in granite); Lo-Apy-Q±Au±Bi,Q-Ccp-Sp, Au-Bsm-sTe (WE veins in hornfels and sandstone)	Py-Apy, Ccp-Sp-Gn, Au-Bi-Se-sAs	Mo-Ms-Q, Apy-Wf-Q, Au-Bi (Bsm, Ik, JoA, JoB, Hed, Bi)
Sulphide content, vol.%	up to 3	up to 3	1-5	up to 2	up to 3	up to 3
Metal signature	W, Au, Bi, Te	Bi, W, As, Cu	Au, Bi, Te	Au, Bi, Te, W	Au, Bi, Te	Mo, Au, Bi
Av. C_{Au}, g/t	~2.5	0.4-1.6	up to 50	up to 50	~2.5	2-5
Au fineness, ‰	672-969	750-980	600-1000	800-850	700-1000	700-950
Age, Ma: pluton/ore	122.3[(1)]/ 124.8±1.5[(7)]	92-97[(1)], 122-124[(4)]/	150.6±1.3[(2)]/	142.9±0.4[(1)]/ 137±3[(1)]		126[(1)]/124.2[(7)]
Stages				1. Au-Bi 2. Ag-Sb	1. Au-Bi 2. Ag-Pb-Zn 3. Ag-Sb	1.Mo (WE veins); 2.Au-Bi (NS veins)
Au resource (Au reserves)**	~30	n/c	n/c	~10	n/c	~5

[(1)]Layer et al., 2001 (Ar-Ar), [(2)]Akinin et al., 2009 (U-Pb SHRIMP); [(3)]Goryachev,2005 (K-Ar); [(4)] Parfenov and Kuzmin, 2001; [(5)] Gamyanin et al., 2015 (Ar-Ar);[(6)] Goryachev, 1998 (Ar-Ar); [(7)]Goryachev, Pirajno, 2014 (Ar-Ar)

Abbreviations: Ank - ankerite, Apy - arsenopyrite, Au – native gold, Bi – native bismuth, Bsm - bismuthinite, Bng - boulangerite, Cal - calcite, Ccp - chalcopyrite, Chl – chlorite, Cos - cosalite, Cs – cassiterite, Gn - galena, Hed – hedleyite, Ik – ikunolite, JoA – joseite A, JoB – joseite B, Kfs – K-feldspar, Lo – löllingite, Ml – maldonite, Mo – molybdenite, Ms - muscovite, PM – polymetallic assemblage, Po - pyrrhotite, Py - pyrite, Q - quartz, sAs – sulphoarsenide, Sch – scheelite, Se – selenide, Sid - siderite, Sp - sphalerite, sTe – sulphotelluride, Tbs – tellurobismuthite, Ttd - tetradymite, Ts – tsumoite, Tur – tourmaline, Wf – wolframite.

*Mineral type: Au-Bi-As - bismuth-arsenide-sulpharsenide deposits, Au-Bi-Te - bismuth-sulphatelluride-quartz deposits, Au-Bi-Sid - bismuth-siderite-polysulphide deposit.

** Au reserves are given in parentheses; n/c – non commercial.

Compiled using Nokleberg et al., 1996; Goryachev, 1998; Gamyanin et al., 2000; Parfenov and Kuzmin, 2001; Gamyanin et al., 2003; Goryachev, 2003; Khanchuk, 2006.

Table 1 (continued).

Deposit	Teutedjak	Shkolnoe	Basugunya	Myakit	Chepak	Dubach
Mineral type*	Au-Bi-Te	Au-Bi-As	Au-Bi-Te	Au-Bi-As	Au-Bi-As	Au-Bi-As
Coordinates (N/E)	61°04´/149°57´	61°28´/149°01´	62°35´/150°58´	61°22´/152°48´	61°58´/148°13´	62°31´/152°40´
Metallogenic belt	Uda-Murgal, K_1	Uda-Murgal, K_1	Yana-Kolyma, J_3-K_1	Yana-Kolyma, J_3-K_1	Yana-Kolyma, J_3-K_1	Yana-Kolyma, J_3-K_1
Pluton/ composition/type	Omchan/granite-leucogranite/ $I_{mgt(?)}$	Burgagy/diorite-granodiorite/ I_{ilm}	Basugunya/ granodiorite-granite /I_{ilm}	Myakit/granite-leucogranite/S	Hidden granitoid pluton	Srednekansk (?)
Rock surrounding pluton	Hornfelsed siltstone and mudstone with single limestone layer (T_3)	Clastic rocks (P_2)	Hornfelsed sandstone and schist (T_3-J_2)	Clastic rocks (T)	Hornfelsed sandstone, siltstone and schist (T_3)	Hornfelsed sandstone and schist (J_1)
Alteration	Skarnification	Greisenisation, beresitisation	Sericitisation	Greisenisation	Greisenisation, silicification, sericitisation	Greisenisation, beresitisation,
Ore location	Contact hornfels and limestone	Apical part of massif	Apical part of massif	Greisens in apical part of massif	Greisens over hidden pluton	Hornfels, dykes
Ore bodies	Stockwork	Veins, stockwork	Veins	Greisens, veins	Greisens, veins	Stockwork, veins
Mineralisation (mineral assemblages)	Skarn with Po, Gn, Sp and Au-Bi (Bsm, Bi, sTe)-Apy-Q	Mo-Apy-Cs-Sch-Q, Py-Apy-Lo, Au-Bi (Bsm, Bi, Ml, sTe)-Apy-Q	Mo-Po-Lo-Apy-Q, Bsm-Ik, Bi-Au-Jo-Hed, Bi-Gn-Cos	sAs (Po-Lo-Bi-Au, Apy-Sp-Ccp-Po), sTe-Bi (Bsm-JoA-Bi-Au, JoB-Hed-Bi-Au)	Apy-Lo-Q, Au-Bi-sTe	Au-Sch-Py-Apy-Bi, Au-Bsm, Au-PM (Gn, Ccp, Sp, Bng)
Sulphide content, vol.%	up to 60 (base metal ores), up to 5 (Au-Bi)	3-5	1-3	up to 10	20-40	4-5
Metal signature	Au, Bi, As, W,	Au, Ag, Bi, Mo, As, Co	As, Bi, W, Mo	As, Bi, Au, Zn	Au, As, W, Bi, Te	Au, As, Bi
Av. C_{Au}, g/t	2.5	3-4	3-4	6.3	7-8	2.6
Au fineness, ‰	650-940	750-859 (up to 1000)	680-940	860-890	880-940	700-850
Age, Ma: pluton/ore	103±2[3]/	150,5±1,2[2]	150±1,6[2]	/141[1]	149[6]/146[6]	/141[6]
Stages	1. skarn base metal 2. Au-Bi-Te	1. Au-Bi-Te 2. Au-Ag-Sb				
Au resource (Au reserves), t**	~50	(50)	n/c	~15	~70	(~35)

Table 2. Microthermometric study of individual fluid inclusions (FI) in quartz from the selected Au-Bi deposits of North-East Russia.

Sample	Inclusion type[1]	n[2]	T_h,°C	T_e,°C	$T_{m\ ice\ (NaCl)}$,°C	$T_{m(CO2)}$,°C	$T_{h(CO2)(N2)}$,°C	Hom. mode CO_2[3]	$T_{m(clatrate)}$,°C	C_{salt}, wt% NaCl equ
						Tuguchak				
150-P-74	III P	8	329-369	-30	-2.2	-	-		-	3.7
	II P	3	385 V	-32	-0.6	-58.8	+3.7	V	-	1.0
	III PS	6	303	-31	-0.7	-	-		-	1.2
156/2- P-74	III P	5	316	-36	-1.2	-	-		-	2.0
	III PS	3	281	-28	-2.2	-	-		-	3.7
161-P-74	I P	3	356	-33	-6.8	-58.6	-8.9	V	-	10.2
	II P	2	-	-	-	-58.2	+6.3	V	-	-
	III PS	22	339-313	-34	-4.6	-	-		-	7.3

	III S	5	265	-32	-3.9	-	-		-	6.3
37-82	III PS	11	231-289	-32…-37	-1.4…-4.6	-	-		-	2.4-7.3
181p74	III PS	14	276-317	-38…-54	-4.9…-25.8	-	-		-	7.7-23.6
174p74	IV PS	7	289	-54	(443)	-	-		-	52.4
	II PS	3	353 V	-30	-3.2	-58.6	9.6	V	9.2	1.6
	II PS	2	-	-	-	-58.2	16.9	L	-	-
	II PS	3	-	-	-	-57.6	23.4	L	-	-
	III PS	4	327	-28	-6.0	-	-		-	9.2
145p74	III PS	23	306-383	-33…-45	-2.3…-3.5	-	-		-	3.9-5.7
						Levo-Dybinskoe				
Ten5	I P	9	268-292	-30…-37	-3.3…-5.1	-57.5	24.8	L	9.8	0.4
	II P	17	-	-	-	-57.5	19.7…24.1	L	-	-
Ten2	IV P	7	411-437	-49	(142-253)	-	-		-	29.3-34.8
	III P	3	351	-45	-6.9	-	-		-	10.4
	I P	2	291	-35	-5.2	-60.3	2.3	L	7.6	5.5
	II P	43	-	-	-	-58.5… -63.1	-2.5…9.4	L-V	-	-
	IV S	4	188	-57	(244)	-	-		-	34.4
	III S	15	183-220	-38…-52	-11.0…-12.9	-	-		-	15.0-16.8
114-79	I P	4	492	-39	-9.0	-57.7	18.1	V	H. o.	11.9
	IV PS	12	384-410	-52…-55	(260)	-	-		-	35.3
	III PS	2	352	-36	-9.9	-	-		6.8	13.8
	I PS	12	349	-33…-40	-7.6…-13.7	-57.4… -57.9	27.1…24.5	V-L	-	11.2
	IV S	3	229	-53	(208)	-	-		-	32.3
	III S	11	222	-37	-6.1	-	-		-	9.3
D114	III, P	25	292-325	-32	-2.5… -5.6					4.2-8.7
	II, P	10				-58.6…-62.7	-58.2…+0.1	V		
	III, PS	15	246-259	-32… -36	-2.3… -2.1					3.6-3.9
							Ergelyakh			
E326*	I P	7	249-286	-30…-36	-2.1…-3.3	-57.8…-58.3	25.7…23.6	L	9.8	0.4
	II P	8	-	-	-	-58.2	20.3…20.9	L	-	-
340-87	IV P	11	254-358	-62	(217-219)	-	-		-	32.7-32.9
	III PS	44	189-285	-29…-36	-2.2…-4.2	-	-		8.9	3.7-6.7
339-87	III P	4	351-341	-32	-4.1	-	-		-	6.6
	III S	6	291	-30	-4.3	-	-		-	6.9
108G-60	III P	6	304	-33	-3.6	-	-		-	5.9
	II P	6	-	-	-	-62.2…-62.5	-11.8…-12.0	V	-	-

	III S	24	264-272	-34…-37	-2.7…-5.5	-	-		-	4.5-8.6
E-114	III PS	9	285	-29	-1.1	-	-		9.4	1.9
	II P	8	-	-	-	-63.0…-62.4	-6.5… -6.0	L	-	-

(1) – inclusion type: 1 – liquid H_2O+ liquid CO_2 ± vapour CO_2, 2 – vapour CO_2-rich (CH_4 rich, N_2 rich), 3 – liquid H_2O+vapour H_2O, 4 - liquid H_2O+vapour H_2O+solid NaCl; P – primary, PS – pseudosecondary and S – secondary inclusions.

(2) – number of studied inclusions. (3) – homogeneous mode of CO_2: L – Liquid, V – Vapor. * – (Au)-Ag-Sb stage, ** – scapolite.

Table 2.(Continued).

Sample	Inclusion type[1]	n[2]	T_h,°C	T_e,°C	$T_{m\ ice\ (NaCl)}$,°C	$T_{m(CO2)}$,°C	$T_{h(CO2)(N2)}$,°C	Hom. mode CO_2[3]	$T_{m(clatrate)}$,°C	C_{salt}, wt% NaCl eq
						Arbatskoe				
26P-74**	IV P	16	650-680	-10	(412)	-	-	-	-	48.5
15Г-82	III P	11	336-342	-32	-2.5… -5.2	-	-	-	-	4.2-8.1
	II P	2	-	-	-	-58.5	-1.6	V	-	-
	III PS	18	299-311	-32… -33	-0.6… -5.2	-	-	-	-	1.1-8.1
						Chuguluk				
Ch-190	III P	9	289	-34	-8.4	-	-		-	12.2
	II P	4	-	-	-	-61.1	-5.9	L	-	-
	IV PS	13	349	-55	(386)	-	-		-	46.0
	IV PS	6	311	-55	(328)	-	-		-	40.4
	II S	2	-	-	-	-62.1	-39.3	V	-	-
	IV PS	5	184	-55	(273)	-	-		-	36.2
	III S	2	205	-41	-3.4	-	-		-	5.6
						Kurum				
Kurum 1	III P	17	282	-23	-3.9	-	-	-	4.2	6.3
(endocontact)	III PS	8	247	-28	-4.2	-	-	-	-	6.7
	III S	5	196-201	-25… -35	-3.1… -4.6	-	-	-	-	5.1-7.3
Kurum-Zh	I P	9	367-374	-25… -33	-	-	-85.9	L	17.6	8.1-9.5
(exocontact)	II P	9	-	-	-	-	-149.2	V	-	-
K-11	I P	24	319-368	-27… -33	-1.3… -5.7	-63.7… -66.0	-7.3… 3.5	V-L	15.5-14.1	1.9-8.8
(500 m from	II P	19	-	-	-	-	-142… -140	V	-	-
contact)	III S	9	258-260	-40...-54	-17.2...-29.7	-	-		-	20.4
	IV PS	15	199-204	-	(181-183)	-	-	-	-	31.0-31.1
K59	III P	3	336	-33	-2.0	-	-	-	-	3.4
	II P	2	334 V	-28	-4.5	-	-88.3	L	-	7.1
	III PS	3	339	-32	-1.9	-	-	-	-	3.2
	II PS	8	-	-	-	-	-88.7	V	-	
13-G-85	III P	12	275-294	-31… -35	-4.0… -4.3	-	-	-	-	6.5-6.9
						Dubach				
Dub2-10	III P	4	248	-30	-3.7	-	-		9.6	5.9
	III P	5	206	-32	-4.2	-	-		8.9	6.7
	II PS	3	-	-	-	-	-118…-77.8	L		-
Dub 511-22	I P	8	254-271	-26	-4.3	-58.5	13.7-21.7	L	10.5	6.8

	II P	4	-	-	-	-58.5	4.0	L	-	-
	II PS	34	-	-	-	-61.8… -63.1	-44.9… +22.9 (-88.6… -100)	V-L	-	
						Basugunya				
B-11	III P	3	284	-32	-5.1				7.3	7.9
	III PS	6	275-252	-32	-2.4				12.6	3.9
						Shkolnoe				
Sh-R-2-1*	I P	3	284	-33	-4.8	-58.6	22.1	V	10.4	6.7
	IIP	5	-	-	-	-59.1…-59.4	11.1…23.9	L	-	
Sh-RT-6-1	I P	16	290-338	-33…-35	-5.7…-6.8	-59.0…-59.8	12.3…15.1	L	10.3-10.8	6.2-8.0
	II P	5	-	-	-	-60.3… -60.6	-14.9…1.2	L	-	-
						Arkachan (after Gamyanin et al., 2015)				
	I P	101	280-385	-31…-49	-16.2…-25.2	-56.6…-58.8	25.4…29.0	V	0.2-10.2	18.8-26.2
	II P	81	-	-	-	-57.3…-59.7	16.5…28.5	L	1.1	-
	III P	11	324-309	-42...-46	-2.2...-5.8	-	-	-	-	3.7-9.0
	III S	36	200-269	-41…-53	-16.4…-23.0	-	-	-	-	19.8-22.6

Table 3. Selected reconstructed fluid compositions for Au-Bi deposits of North-East Russia according to crush-leach analysis.

Deposit	Levo-Dybinskoe	Chuguluk	Ergelyakh	Chepak	Dubach	Teutedjak	Shkolnoe	Tuguchak	Kandidatskoe	Kurum	Chi
Sample	179-gr-79	190-g-61	332-g-87	chep-3-2	dub-8-19	93p-teu	rt-6-1shk	37-G-82	134-g-82	12-G-90	Chis-0
CO_2, $^x10^3$ ppm	43.39	153.3	95.31	7.54	28.87	13.82	91.10	32.65	2.68	5.87	1
CH_4	1.58	10.12	25.57	14.83	30.17	0.33	6.98	0.99	0.31	5.68	1
Cl^-	45.92	4.57	32.34	11.62	21.37	13.83	9.29	20.47	3.82	9.93	0
SO_4^{2-}	2.87	73.24	-	-	-	-	-	-	-	-	
HCO_3^-	-	0.10	4.50	1.08	1.61	0.04	2.04	25.24	8.22	31.70	0
F^-	-	-	-	-	-	-	-	-	-	-	
Na	23.08	11.38	13.02	4.86	9.27	4.22	4.75	20.22	4.60	8.57	0
K	3.65	6.46	1.41	0.38	2.77	1.67	0.46	2.90	0.86	2.23	0
Ca	2.03	2.57	7.78	2.57	2.71	2.90	1.53	0.75	0.27	6.42	0
Mg	-	0.05	0.08	0.01	0.33	0.10	0.05	0.09	0.10	0.63	0
Br, ppm	123.7	-	85.49	-	-	-	-	7.55	65.30	-	26
B	73.1	133.8	118.4	45.7	588.7	141.5	86.4	220.7	699.6	1245	1
Li	-	251.5	4.80	0.27	139.2	5.27	1.06	6.96	35.33	33.72	43
Rb	43.64	11.53	12.52	2.94	5.64	6.16	2.19	34.38	1.02	9.84	3
Cs	55.49	6.51	23.82	11.41	17.87	3.69	1.54	19.88	0.13	4.50	0
Sr	141.5	2478	462.7	83.43	50.82	26.85	63.86	20.11	1.93	92.96	25
Ba	12.24	18.04	193.9	5.31	1.81	18.82	8.87	44.30	9.01	48.54	1
As	176	24884	497	1092	3821	50	116	556	476	47	
Sb	333	287	414	127	808	333	123	8.8	34	3.30	
Ge	0.14	0.29	0.47	0.37	2.23	0.20	0.72	0.10	0.13	0.22	
Cu	-	-	-	4.39	1.97	-	0.71	2.07	-	4.01	46
Zn	297.5	48.43	-	3.79	-	252.7	-	332.3	-	421.6	16
Cd	1.37	15.99	3.07	0.05	0.02	0.53	0.01	1.04	0.02	-	0
Pb	4.18	1.04	6.64	0.59	4.32	-	-	-	0.32	-	1
Au	0.01	-	-	-	-	0.14	-	-	0.02	0.13	
Ag	-	-	0.11	0.13	0.02	0.74	0.06	-	-	-	0
Bi	18.06	-	-	-	-	-	1.98	0.48	0.04	-	
Mo	0.07	-	1.20	0.03	0.07	-	0.16	0.45	1.98	0.30	0
W	14.02	-	0.92	8.38	12.89	0.01	0.63	2.65	1.35	0.09	1
Sn	0.54	-	-	-	-	0.28	-	12.45	-	-	0
Hg	-	-	-	-	0.19	-	0.14	-	-	-	1
Tl	0.21	2.04	0.15	0.02	0.28	0.30	0.21	0.15	0.08	0.28	0

Co	0.23	0.02	0.06	0.15	-	2.04	0.07	0.39	0.01	0.17	0
Ni	10.13	7.96	4.11	2.82	1.06	17.57	0.17	6.97	0.24	5.00	16
Cr	-	-	-	0.39	2.54	-	-	0.12	0.30	-	
V	-	-	-	-	-	-	-	0.40	2.06	-	
U	-	0.11	-	-	-	-	-	-	-	-	0
Mn	193.9	1.48	259.4	5.70	4.27	-	-	302.6	1.76	27.03	13
Fe	40.74	4896	-	28.58	-	-	-	4.63	12.19	38.53	58
Th	0.01	-	-	-	-	-	-	-	-	-	
Si	4446	-	-	146.2	1679	-	318.6	-	1913	-	

- Below detection

Table 4. PTX-parameters of fluids and stable isotope composition of minerals for the Au-Bi deposits of North-East Russia.

Deposit	Megastage	Fluid inclusion (FI) data				Stable isotope data		
		FI type[(1)]	T,°C	Salinity, wt % NaCl equiv	P, kbar	$\delta^{18}O_{SMOW}$, ‰	$\delta^{13}C_{PDB}$, ‰	$\delta^{34}S_{CDT}$, ‰
Tuguchak		I, II, **III**, IV	385-231	1.0-52.4	0.3-0.4	12.7 *Q*		-8.0…-6.0 *Apy, Mo*
Levo-Dybinskoe		I, **II**, III, IV	492-183	0.4-35.3	0.1-1.3	8.3…11.2 Q_γ 10.8…13.1 *Q* 13.9…14.0 *Ca*	-7.3…-7.1	-1.8…+0.8 *Apy, Py, Po*
Ergelyakh	Q-Wf	II, III	304-264	4.5-8.6	0.2	8.2…8.7 Q_γ 3.1 *Wf*		
	Au-Bi	**III**, IV	358-189	1.9-32.9	-	11.9-13.6 *Q* 2.1…5.7 *Ca*	-6.9…-5.9	-6.7…-0.3 *Apy, Py, Po*
	Ag-Sb	I, II	286-249	0.4	0.9-1.1	13.3…13.6 *Q* 2.3 *Ca*	-11.6	
Arbatskoe	skarns	IV	680-650	48.5	-			
	Au-Bi	II,**III**	342-299	1.1-8.1	0.2			
Chuguluk		II, III, **IV**	349-184	12.2-46.0	1.4	9.1…10.5 Q_γ 12.6-13.2 *Q*		-13.9…-12.8 *Apy, Po*
Kurum		**I**, **II**, **III**, IV	374-196	3.2-31.1	0.4-1.4	8.0…8.9 Q_γ 10.3…13.3 *Q*		-6.7…+0.2 *Apy, Py, Po,Gr*
Dubach		I, **II**, III	271-206	5.9-6.8	1.8-1.9	12.2…13.1 *Q*		-12.2…-7.0 *Apy*
Basugunya		III	284-252	3.9-7.9	-	12.2 *Q*		-12.5…-9.6 *Apy*
Shkolnoe	Au-Bi	**I**, II	338-290	6.2-8.0	1.3-1.9	11.8 *Q*		-8.8…-5.3
	Au-Ag-Sb	I, II	284	6.7	0.1-1.1	16.2 *Q*		*Apy, Py, Sp*
Arkachan	Au-Bi	**I**, II, III	385-200	3.7-26.2	1.1-1.8	13.6-15.4 *Q* 13.6-15.5 *Ca*	-6.0…-3.6	-1.9…+16.0 *Apy, Py, Sp, C*
	Ag-Pb					16.3 *Q*		
	Ag-Sb					8.9-9.4 *Q*		
Teutedjak		I, II, IV	473-318	13-45.9	0.8-0.9*			0…+1.6 *Apy*
Chistoe						10.6-12.1 *Q* 0.3 *Ca*	-6.8	-10.6…-7.5 *Apy*
Kandidatskoe						11.7 *Ca*	-4.5	-8.5…-7.3 *Apy*
Delyankir						12.1…12.3 *Q*		-7.0 *Apy*
Chepak						13.4…15 *Q*		-11.7…-4.9 *Ap*
Myakit								-18…-9.9 *Apy*
Galechnoe						10.6…12.0 *Q* 3.0 *Wf*		+4.4…+4.6 *Ap*
Nenneli						14.4 *Q*		-5.5…-1.3 *Apy, Sp, Ccp,C*

[(1)]– Inclusion type: I – liquid H_2O+ liquid CO_2 ± vapour CO_2, II – vapour CO_2-rich (CH_4 rich, N_2 rich), III – liquid H_2O+vapour H_2O, IV - liquid H_2O+vapour H_2O+solid NaCl, bold – most common.
[(2)] – Na/K geothermometer, Díaz-Gonzáles and Santoyo, 2008; [(3)] – Fe/Mn geothermometer, Pester et al., 2011; [(4)] – Si geothermometer, Fournier and Potter, 1982; in parentheses – number of analyses.
* data from Struzhkov et al., 2008.
Abbreviations: Apy - arsenopyrite, Ca - carbonate, Ccp - chalcopyrite, Gn - galena, Mo – molybdenite, Po - pyrrhotite, Py - pyrite, Q - quartz, Q_γ - quartz from granitoids, Sp - sphalerite, Wf – wolframite.

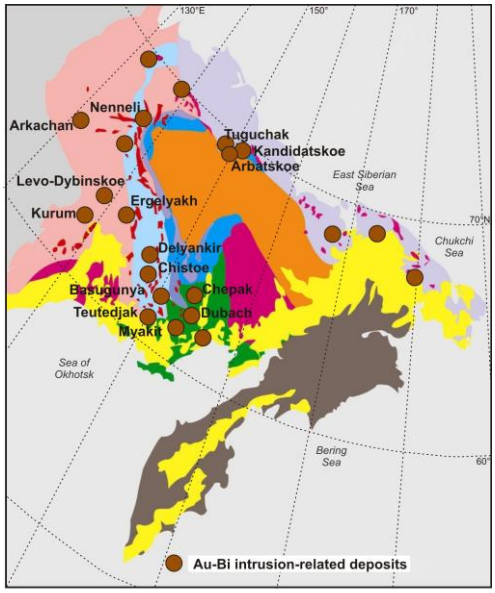

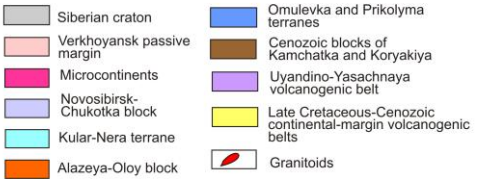

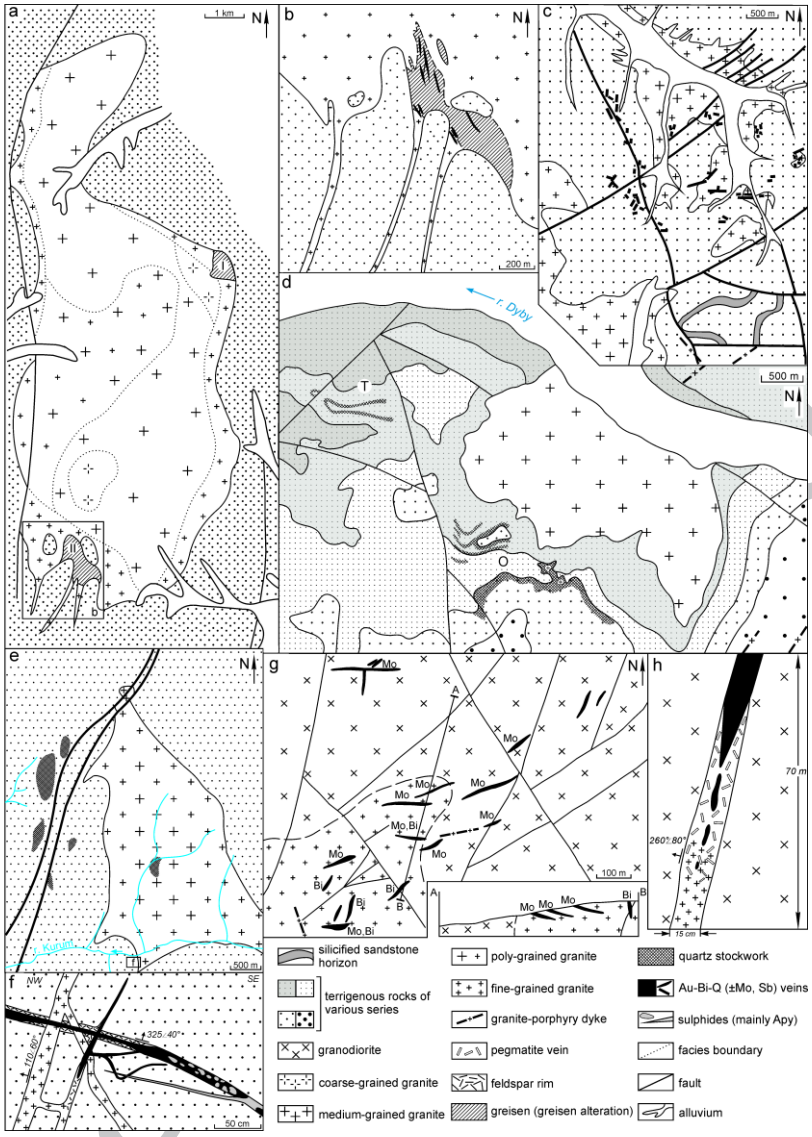

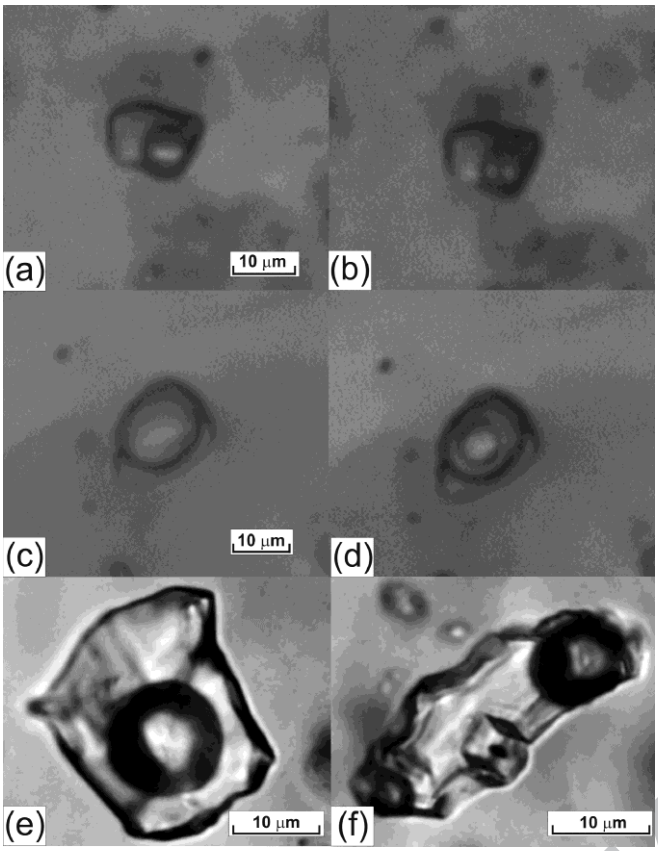

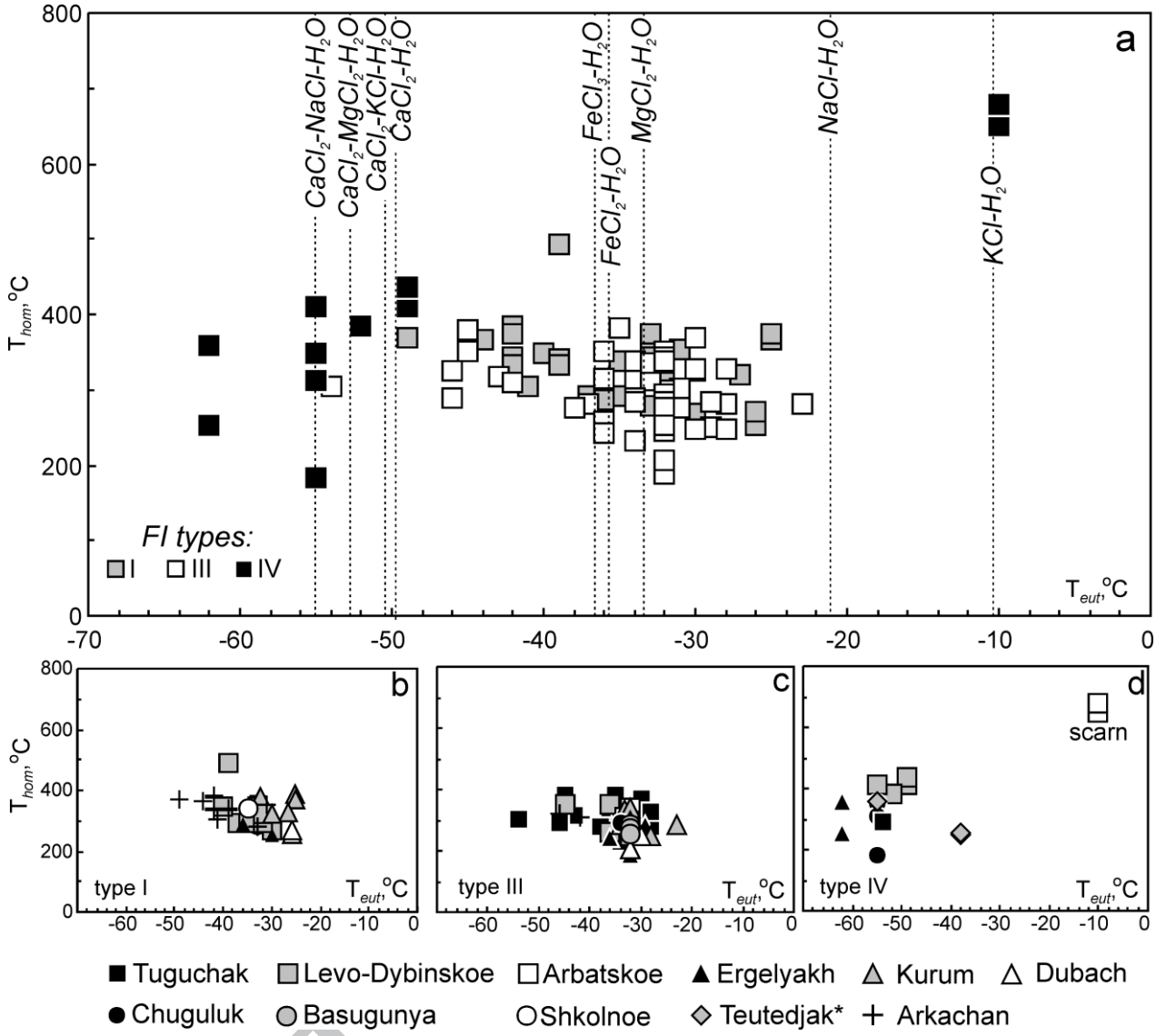

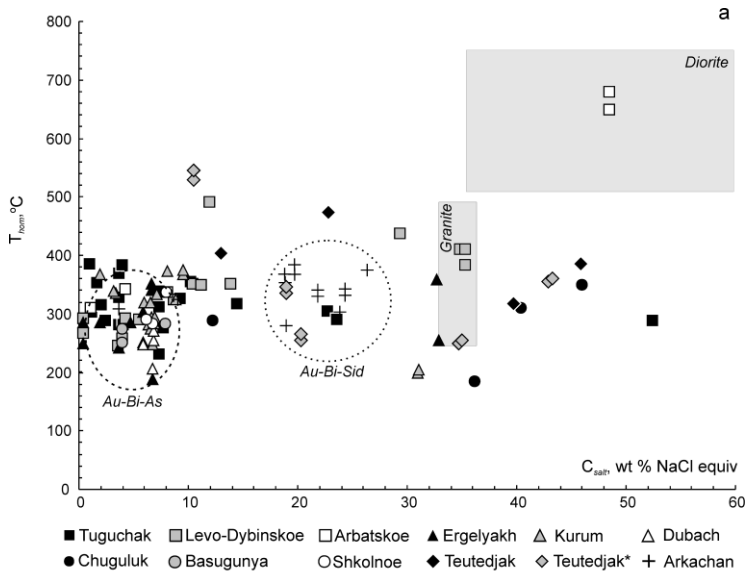

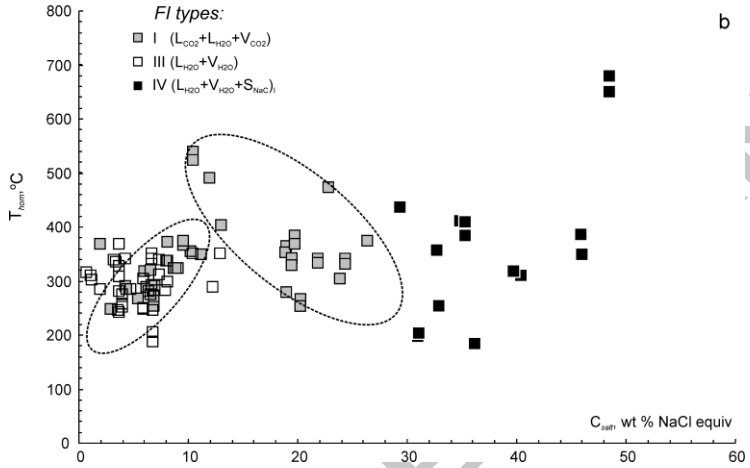

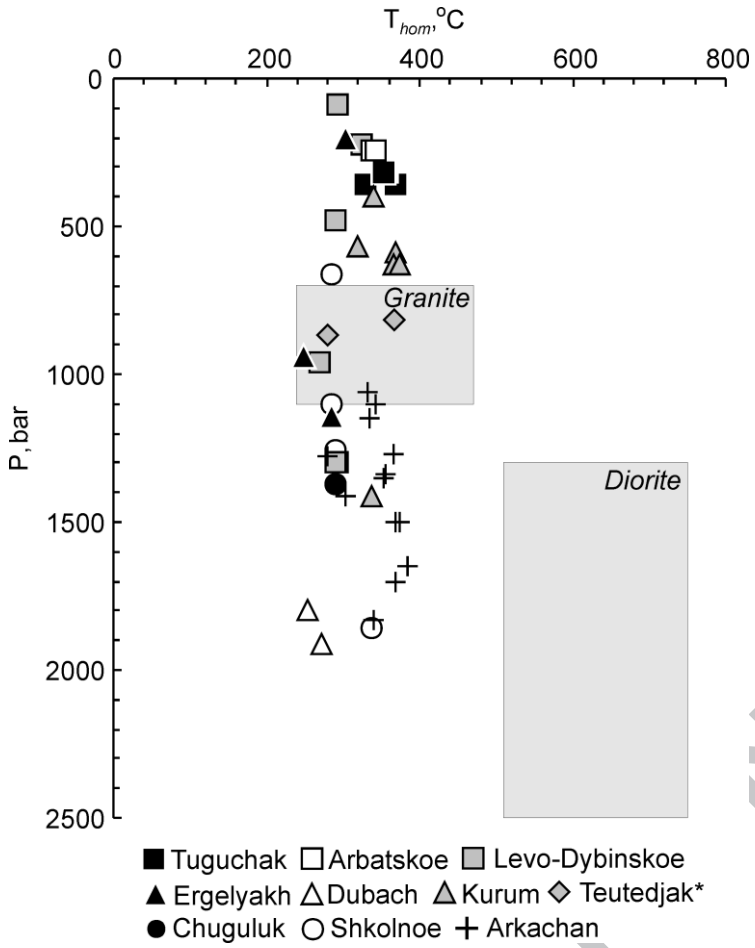

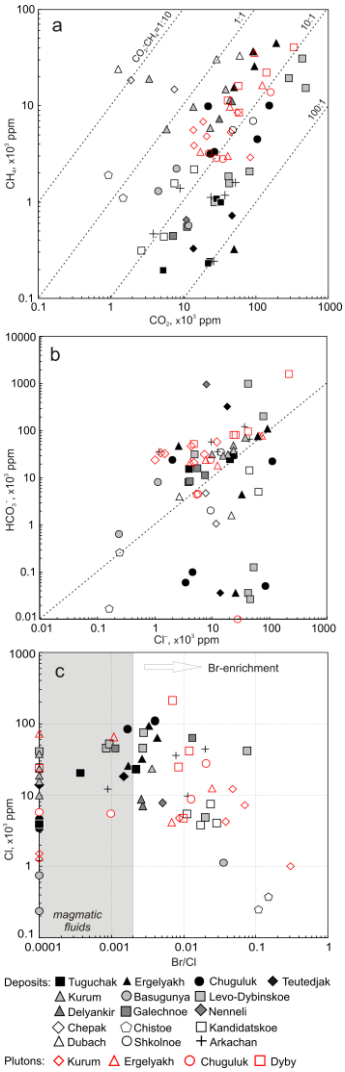

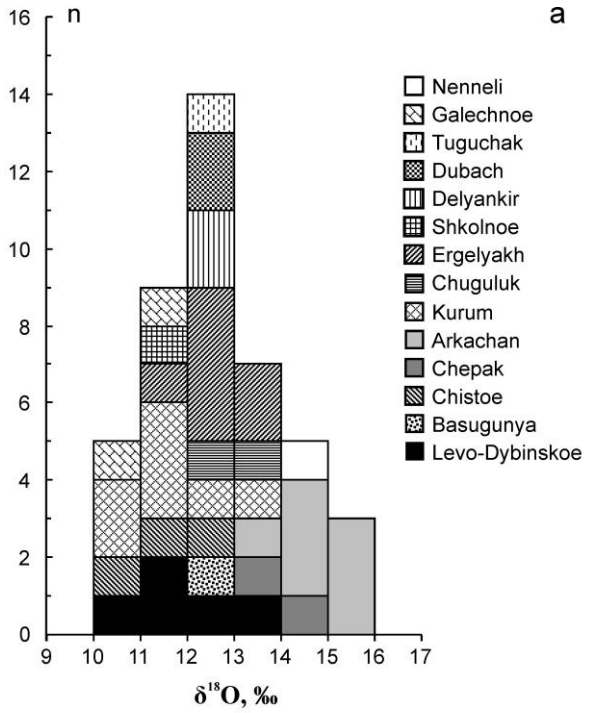

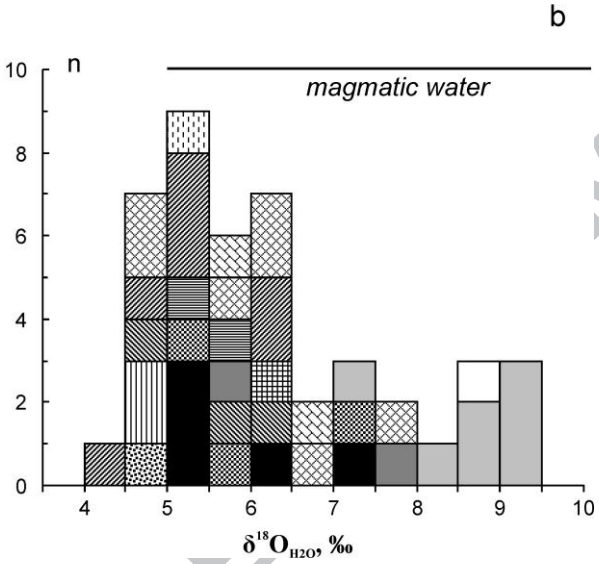

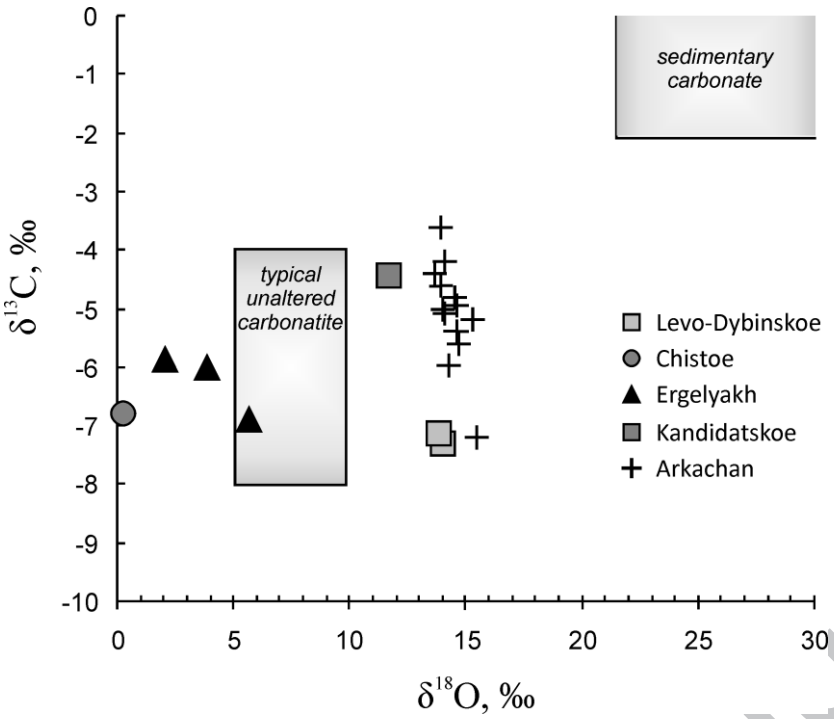

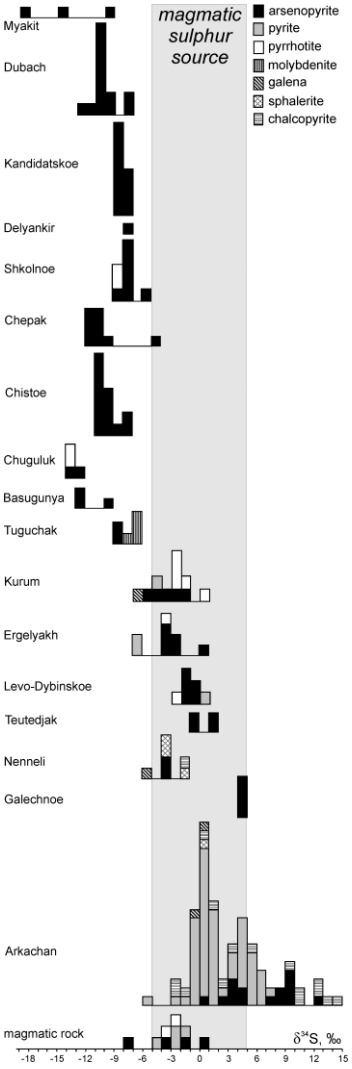

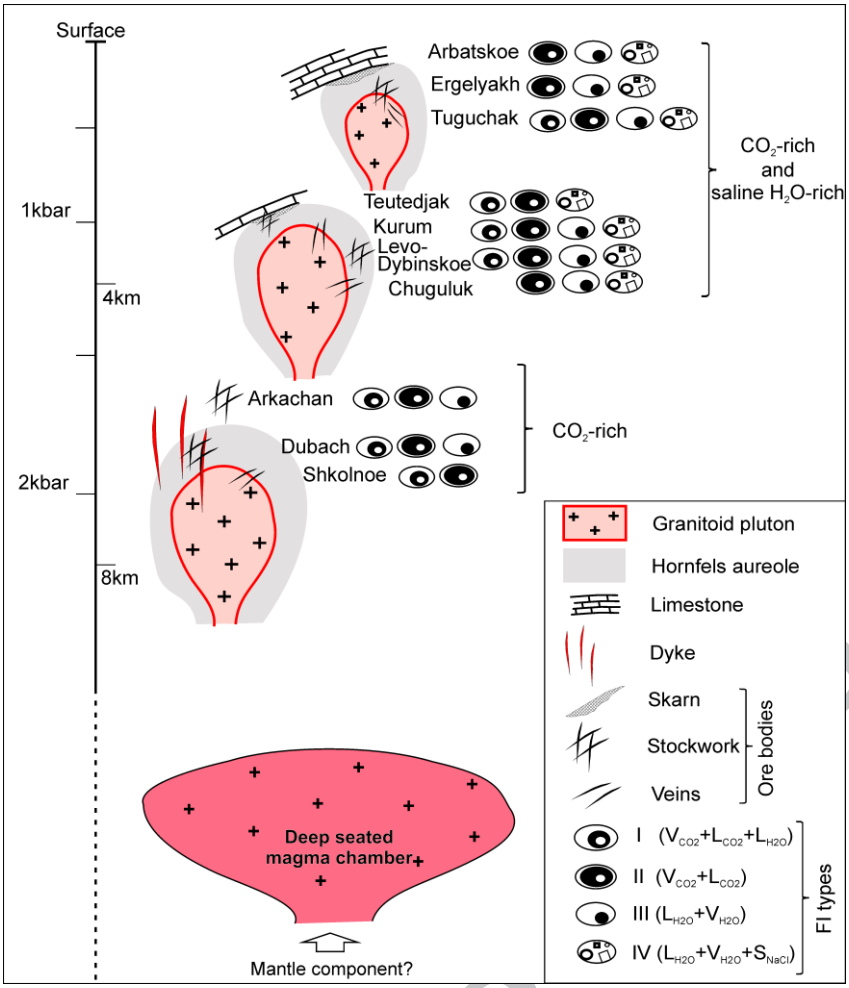

PTX and stable isotope data for eighteen Au-Bi intrusion-related deposits of North-East Russia were summarized.

Au-Bi mineralisation was formed at 437 to 200°C (mainly from 400 to 250°C) and 0.1 to 1.9 kbar from H_2O-CO_2-NaCl fluid.

Brine and CO_2-rich inclusions coexist in deposits at shallow depth, presence of CO_2-rich inclusions and lack of brines occur at deeper level.

Stable isotope data suggest predominantly magmatic source of gold-bearing fluids but magmatic fluid was enriched with light O, C and S isotopes as a result of fluid immiscibility.